Combining Multi-Wavelength AERONET SSA Retrievals with a MIE Model to Quantify the Size of Absorbing Aerosols and the In-Situ Lifetime of Sulfate

Xinying Wang[1], Jason Blake Cohen[2*], Shuo Wang[3]

[1]School of Atmospheric Sciences, Sun Yat-Sen University, Guangzhou, China.

[2]School of Environment and Spatial Informatics, China University of Mining and Technology, Xuzhou, China.

[3]School of Electronic Engineering, Chengdu University of Information Technology, Chengdu, China.

Corresponding author: Jason Blake Cohen (jasonbc@alum.mit.edu)

Key Points:

- Urban sites throughout Asia are impacted not only by local sources but also biomass burning and sources conveyed long-range transport.
- Quantifies the age and attributes the sources as a function of time based on multiple wavelength analysis.
- Uncertainty analysis indicates that the number of very small particles and total absorbtion are underestimated by surface measurements.

Abstract

Energy, transport, urbanization and burning are responsible for changes in atmospheric BC. This work uses direct solar atmospheric column measurements of single scatter albedo [SSA] retrieved at multiple wavelengths from AERONET at 68 Asian sites over 17 years. A MIE model is solved across the wavelengths using a core-shell mixing approximation to invert the probabilistic BC, shell size, and UV SSA. Orthogonal patterns are obtained for urban, biomass burning [BB], and long-range transport [LRT] conditions, which are used to analyze and attribute source types of BC across the region. Large urban areas (thought to be dominated by urban BC) are observations during targeted times (shorter than seasonally) to yield significant contributions from non-urban BC. BB and LRT are observed to dominate Beijing and Hong Kong 2 months a year. LRT is observed during the clean Asian Monsoon season in both Nepal and Hong Kong, with sources identified from thousands of kilometers away. Computing the shift in shell size required to constrain the results approximates secondary aerosol growth in-situ, and subsequently aerosol lifetime, which is found to range from 11 days to a month, implying both a significant amount of BC above the boundary layer, and that BC generally has a longer lifetime than PM2.5. These findings are outside of the range of most modeling studies focusing on PM2.5, but are consistent with independent measurements from SP2 and modeling studies of BC that use core-shell mixing together with high BC emissions.

Plain Language Summary

Energy, transport, urbanization and burning are responsible for significant changes in atmospheric Black Carbon aerosol [BC]. This study analyzes atmospheric column measurements

using different parts of the solar spectrum with a physical model, to describe the solution set of BC and coating sizes in the atmosphere. This information is then used to make different aerosol types, including urban, biomass burning, and aerosols which have been in the atmosphere for a very long time. These type profiles are applied throughout Asia to analyze the sources of BC. While many sites are as expected, most large urban areas are observed to have both biomass burning and long-range transport types found when looking over short time periods which occur annually. Next, even during heavy Monsoon rains, urban areas are found to have significant amounts of long-range transported BC. The lifetime of the BC is also obtained from the growth in the shell size, demonstrating that BC stays in the atmosphere longer than current studies focusing on PM2.5 can observe. Focusing models more specifically on BC, formulating different controls during different periods of the year, and better studies of BC emissions could all yield improved understanding of BC and its effects.

1 Introduction

Black carbon (BC), organic carbon (OC) and dust (or Absorbing Aerosols - AA) can strongly interact with solar radiationi, leading to impacts on the atmospheric radiation budget, climate, water cycle, and more (Jacobson, 2001; Menon et al., 2002; Wu et al., 2008). Black Carbon can absorb solar radiation strongly in the visible and infrared. Small changes in BC loadings can cause a significant change in the local solar radiation absorption and hence altering the regional and global climate (Ramanathan et al., 2001a, 2001b). This interaction critically relies on the particle size distribution, chemical composition and mixing state in-situ (Jacobson, 2001). The two most significant difficulties in estimation of the climate effects of black carbon are the variable physical-chemical properties of BC-containing particles (Miyakawa et al., 2017) and the heterogeneous distribution (Bollasina et al., 2013; Shen Z et al., 2020; Cooke et al., 2002; Lu et al., 2011). While BC itself is water-insoluble once it has been in the atmosphere for a long enough time, it will become coated (Zhang et al., 2016; Cohen and Wang, 2014) in turn becoming hygroscopic (McMeeking et al., 2011) and therefore having the potential to impact climate via wet and ice clouds (Penner et al., 1992; Penner et al., 2001; Kuwata et al., 2007). Due to its long lifetime in the atmosphere, BC has also been known to travel very long distances, impacting regions thousands of km away from the source region, and underging in-situ processing such that it's absorbance and impact on clouds may both be enhanced, further impacting the radiative balance over large scales (Liu et al., 2011; Zhang et al., 2015; Prasad et al., 2018; Guha et al., 2015; Wang et al., 2009). Taking all of these factors into consideration, the current range of radiative forcing estimates of BC (at TOA) range from +0.13 to +1.4 W/m^2 (Haywood and Shine, 1995; Haywood et al., 1997; Haywood and Ramaswamy, 1998; Myhre et al., 1998; Penner et al., 1998; Cooke et al., 1999; Jacobson, 2000; Wang, 2004; Wang et al., 2014; Jacobson et al., 2001; Bond et al., 2013; Cohen et al., 2011).

Attempts have been made to elucidate particle size, mixing state, emissions, and aging over highly polluted regions in Asia using different models and methods (Salam et al., 2012; Quinn et al., 2004; Kompalli et al., 2021; Han et al., 2013; Streets et al., 2003; Kühn et al., 2014; Xu et al., 2015; Song et al., 1999). However, at the present time there are few if any studies that have comprehensively focused on the long-term properties of the particle size and source (i.e. distance to a biomass burning or urban source) and aging (i.e how long the aerosol has undergone processing and deposition in-situ). Studies which have analyzed aerosols using remote sensing have tended to focus on the visible and IR radiative bands, with measurements from the UV band scarcely used (Corrigan et al., 2006). In specific, many present remote sensing

based studies merely focus on a fine mode and coarse mode (Eck et al., 2010; Koulouri et al., 2008; Zhang et al., 2017; Kleidman et al., 2005). Attempts have also been made via field observations. Schwarz et al (2008) used an airborne single-particle soot photometer to quantify BC aerosol microphysical state in fresh urban and BB emissions. These differences contribute to significant impacts on the BC size distribution and concentration, when observed using measurements based on particulate absorption (Sato et al., 2003). However, results such as these from both remote sensing and field studies are not considered in most chemical transport and aerosol models today, which tend to not assume a Core-Shell approximation which in turn tends to underestimate the overall absorption profile, requiring scaling to match optical properties such as SSA, AAOD and size information (Myhre et al, 1998; Cooke et al.,1999; Jacobson et al., 2000; Wang et al., 2009; Cohen et al 2011). Consequently, these models tend to underestimate ultra-long-range transport and non-local polluted conditions, frequently induced by vertical transport and aging associated with underestimated absorption (Wang et al., 2020). It has been demonstrated that a Core-Shell model fits best with aerosol properties in heavily polluted region such as East, Southeast and South Asia where sulfate or nitrate can coat on BC in a short time after it has been emitted, consistent with the fact that in these parts of the world biomass burning sources and urbanization are located in close proximity to each other (Cohen and Wang, 2014; Peng et al., 2016; Zhang et al., 2016; Cohen et al., 2017).

To achieve a better understanding of AA and its impact on the atmosphere, this work incorporates multi-spectral atmospheric column high frequency measurements and inversion products from AERONET including AOD and SSA, as well as mixing state and size measurements from ground station, in connection with a inverse constrained variance maximation approach to reveal size and absorbtion properties of aerosols in Asia. A specific focus is made on the added value of using measurements in the UV bands which provides deeper support for and quantiatiave insight into the loadings and sizes of smaller particles, allowing for better characterization of both aging as well as fresher particles. The inversely constrained particulate core and shell sizes based on the SSA valuess from the Mie model and constrainted by AERONET, allow for a new categorization of aerosols aerosols based on whether they are emitted locally in Urban areas [Urban], have undergrone Long-Rang Transport [LRT], or are emitted locally by Biomass Burning [BB]. The approach also allowes a stastitical solution space to indicate the range of mixtures of these source types which would also be capable of being physically realistic, taking into the specific particle size (both core and shell) distribution. This allows the use of typical and well classified sites to be used to improve understanding of different sources and their contributions to the atmospheric loading, as well as impacts on radiative forcing and subsequently on climate change. Since these are based on column measurements of the entire atmosphere, they provide important support to further promote improvement of models, in terms of capturing the total atmospheric loading, attirubiton of extreme or abnormal events, and impacts of high-frequecy changes on the overall performance of models, all of which are cited as important weaknesses of current aerosol modeling systems. Some specific scientific points of interest discovered include quantification of significant events in which mixing occurs between an expected and an unexpected source, detection of missing/previously unidentified sources, details about changes in the optical and size poperities of aerosols which are otherwise obscured when only looking at a $PM_{2.5}$ or Fine Mode type of aerosol constraint, and quantifying of different aging rates occuring between BB and Urban cases. It is finally hoped that ongoing calculations incorporating the quantitative approach explicitly employed here will allow for further expansion and insights to be gained and for more

multi-wavelength measurement platforms of aerosol absorbtion to be further incorporated in the future, allowing for further understanding, advances in attribution, and improvement of models and impacts on people, health, and the climate system.

2 Data and Methods

2.1 AERONET Data

This work uses Aerosol Optical Depth (AOD) and Single Scattering Albedo (SSA) from March 1997 to May 2017 using ground-based Aerosol Robotic Network (AERONET) observations. AERONET uses CET318-TS9 instruments to provide information about the spectral sun irradiance and sky radiances at multi-bands including at wavelengths of 340 and 380 (AOD only), and 440, 670, 870 and 1020nm (both AOD and SSA) (https://aeronet.gsfc.nasa.gov/new_web/data_description_AOD_V2.html). This work uses level 2.0 cloud screened and quality assured data (Holben et al., 2006), focusing on the time variations and loading/magnitude of the daily mean measurements over the entirety of the time series which have three or more individual measurements available within the time of one calendar day. To avoid the case where there is a weak signal and ensure sites have sufficient data to capture the feature of each site, all AERONET sites were filtered previous to classification, only retaining sites that have 100 or more days of data in addition to at least one of three conditions: high mean AOD, high extreme event AOD, or highly variable AOD. If a site has more than 300 days of total data (Wang et al., 2021; Dubovik and King et al., 2000; Dubovik et al., 2002), then the site is also used, even if it does not meet one of the three conditions. After filtering 68 sites remain for further analysis throughout East Asia, Southeast Asia, South Asia, Eastern Russia, and Australia. Furthermore, other than sites located in Western India and Western China, the remainder of the sites in this analysis do not generally have a significant dust loading, and therefore the major source of absorption is assumed to be black carbon (BC), allowing this work to assume a direct relationship between BC and SSA (Cohen and Wang, 2014).

2.2 Mie Model

A Mie model is used to connect the radiative measurements and observations from AERONET with approximations of the various optical, mixing state, and implied chemical properties of the aerosols. Mie Theory solves the aerosol optical properties based on a given size and optical distribution of particles, following Bohren and Huffman (1983). It assumed the time variation of the field is $\exp^{-i\omega t}$, leading exclusively to positive imaginary parts of the refractive index corresponding to absorbing media. Although externally, internally and core-shell mixtures are frequently used characterize particle morphologies and chemical compositions (Cheng et al., 2008; Lin et al., 2013; Tao et al., 2019; Zhang et al., 2017), this work assumes that all the particles have a Core-Shell structure, which has been demonstrated to be reasonable in urban areas in Asia based on both modeling and measurement studies (Cohen et al., 2011; Cohen and Wang, 2014, Zamora et al., 2019), as well as being compatible with the AERONET inversion technique (Dubovick, 2002).

Using particle size and refractive indices, this work computes the extinction coefficient (Qext), scattering coefficient (Qsca) and absorbing coefficient (Qabs). The resulting single-scattering albedo (SSA) is calculated based on the equation (1) (Hansen et al., 2009).

$$SSA = \frac{SCATTERING}{EXTINCTION} = \frac{Q_{sca}}{Q_{ext}} \#(1)$$

Since AERONET does not report the SSA in the UV band, this work computes the SSA field using the MIE model at 340nm using a core-shell approximation where the aerosols contain a pure BC core with a scattering (i.e. Sulfate or Nitrate) coating, where the core refractive index is 2.0+1.0i (Schuster et al., 2005) and the shell refractive index is $1.52\text{-}5*10^{-4}$i (B Aouierats et al., 2010). This is physically consistent with the facts that many primary aerosols in these regions are organic and that they age rapidly as a function of their time in-situ (Cohen and Wang, 2014; May et al., 2015; Song et al., 1999). The model computes particle sizes of the core in steps of 0.01μm from 0.05μm to 0.50μm, and the shell in steps of 0.01μm from 0.01μm to 0.80μm.

2.3 Copernicus Atmosphere Monitoring Service (CAMS) SO_2 data

CAMS global reanalysis product provides monthly average SO_2 at 0.75°x0.75° resolution (https://ads.atmosphere.copernicus.eu/cdsapp#!/dataset/cams-global-reanalysis-eac4-monthly?tab=overview). This study uses data from 2019 data over 7 vertical levels from the surface to 700hPa. Additional measurements of SO_2 at the surface are obtained over China from the Ministry of Ecology and Environment of the People's Republic of China.

2.4 Single Particle Soot Photometer (SP2) Measurement

SP2 measures individual aerosol particles. These measurements are capable of determining the optical size and characteristics by scattering and absorption using 1040nm radiation, as well as induced laser incandescence of pure carbon-containing cores. In the real atmosphere at these wavelengths, the major source of absorption corresponds to BC (Bond, T.C., et al., 2013; Bond and Bergstrom, 2006; Bond, 2001; Penner, 1994), which can then be converted into a core diameter (Dc) using a mass equivalent diameter (ρ=1.8g/cm^{-3} for atmospheric BC) and assuming that BC is spherical (Martins et al., 1998; Smith and Grainger, 2014; Jacobson and M.Z., 2000, 2001). The optical diameter of the non-BC portions of the particle (Dp) is calculated using Mie theory, and presented as (Dp/Dc).

This study used SP2 data measured by the Institute of Atmospheric Physics Beijing (39.58'28''N, 116.22'16''E) observed from 2016.11.10 to 2017.09.15. This specific location is located very close to an AERONET station in Beijing (39.977N, 116.381E) which has measurements in 2001 (March to May), 2015 (September to December) and 2016 (January to July). The is an overlap between these two datasets from 2016.11.10 to 2017.01.12, which hereafter is used for the comparison between Dp/Dc inverted from AERONET and measured by SP2.

2.5 In-situ lifetime calculation

Considering that a minimum concentration of sulfuric (or nitric) acid is required before BC can age, the lifetime of SO_2 provides an excellent proxy to approximate the time in-situ. This can be quantified following Equation 2 where M is the SO_2 concentration, and k is the rate constant.

$$\frac{D[M]}{Dt} = -k[M]\#(2)$$

The solution of Equation 2, after rearrangement of the terms is given in Equation 3 where k equals to t/τ, t is the in-situ time the particle spent in the atmosphere, τ is the e-folding time of SO_2 in-situ, M(env.) is the mean environmental concentration of SO_2 encountered by the particle, and M(growth) is calculated based on the [BB] Profile (more details in 4.1), based on the average atmospheric concentration of sulfate in the region studied being about 2.9ug/m^3.

$$t = \frac{-ln\frac{M(growth)}{M(env.)}}{\tau} \#(3)$$

In the background case, the assumed lifetime of SO_2 is 1.56 days (Pham et al., 1995; Chuang et al., 1997; Chin et al., 1996; Croft et al., 2014; Restad et al., 1998). In the urban case, the lifetime is expected to be shorter, since the loading of OH is higher and coversion to H_2SO_4 gas and subsequent gas to particle conversion is faster (Cohen et al., 2011; Liu et al., 2018; Saiz-Lopez et al., 2017; Saxena et al., 1987). This work recalculates the e-folding time assuming that Beijing is a representative site for urban chemistry. Based on the Beijing high time profile obtained by extracting the size value in the peak period (25 days in total) and the ground measurements of SO_2 from the China EPA Beijing station, the urban lifetime is computed to be approximately 0.98 days.

2.6 Statistics and analytics used in this work

Considering that many sites in the region are undergoing rapid change and might have different characteristics during different time periods, a method is derived to look at extremely polluted days separately from the non-polluted days. This selection of heavily polluted days is made by defining the peaks of the data greater than the mean plus one standard deviation, removing these, and re-iterating 3 times. The net aggregation of those days is herein considered heavily polluted.

3 Analyses of selected regions

3.1 Time series of selected cases

The temporal characteristics of daily average AERONET AOD (340nm) over different times are given in Figure 1, with non-polluted values shown in green, while those considered heavily polluted are uniquely represented as blue, black, and red respectively based on being filtered during the first, second, and third passes respectively. Common features observed include relatively regular signals of an annual peak and trough with a roughly similar start time, end time and duration. Some sites occasionally have large values and otherwise are relatively low or moderate in terms of AOD, but without any clear pattern (these patterns do not have any clear start or end time, duration, magnitude, or extremum), leading to the changes being associated with some process that locally varies significantly from time to time, consistent with long-range transport based events. In these cases, the average AOD during the non-peak times tends to be not high. In addition to the above situations, sometimes the distribution of AOD is completely irregular, with no obvious pattern during either the cleaner periods or the peak periods, and no obvious pattern in terms of high or low magnitude. In this case, the source region is more likely to be urban in nature, because urban emissions exist year-round without a large amount of variation, although small changes due to the day of the week, the season of the year, and local meteorology combine to provide temporal variability.

Chiangmai is the biggest city in northern Thailand and is the only location in Northern Thailand, Myanmar, or Laos with an industrial presence (population of 127,000). However, based on previous work (Lin and Cohen et al., 2020; Wang and Cohen et al., 2020; Cohen et al., 2017), this region generally has industrial and urban signals of emissions which are very small, instead having a signal dominated by biomass burning. Based on Figure 1a, the time series of

Chiangmai has a very unique feature with most of the year being relatively clean, and a short but intense time during which it is extremely polluted. The peak always occurs during roughly the same time (From February through 19 April) every year over the entirety of the 10 years of measurements, and furthermore a peak never occurs outside of this time. Given this and the previous works identified above, Chiangmai is considered the most representative region with respect to biomass burning.

Taihu is a large lake located partially in Wuxi (7 million people) and partially in Suzhou (11 million people), cities which have the second and third highest per capita PPP in China. The lake is located in the middle of the Shanghai, Nanjing, Hangzhou conurbation. For this reason, the region has a huge amount of individual vehicles, factories, manufacturing and other economic activity, yet is not adjacent to any specific road or factory. As such, it is quite representative of a region in which the major source of pollution is urban, as has been shown by previous works (Huang et al., 2021; An et al., 2021; Logan et al., 2013; Chen et al., 2020). As shown in Fig. 1(b), a time series of the AOD tends to be high on average, and contains a large amount of variability that appears both random and not intensely concentrated during any specific periods of time.

Palangkaraya is a small city located in southwestern Borneo, which is surrounded by forests and peatlands. The city itself is not a major source of emissions, and while the surrounding land had been frequently burned in the past, today it consists of plantations without any more burneding. The data available at this site ranges from 2012 through 2016, during which the location region was already transformed into plantation (nearly no local sources), but which was surrounded by generally high amounts of biomass burning hundreds to thousands of kilometers away coming from elsewhere in the Maritime Continent in 2012 and 2015, as demonstrated by the time series data itself, and previous studies (Deng et al., 2020; Cohen, 2014). The relatively low mean and high standard deviation of AOD show a consistent pattern whereby the region is impacted by long-range transport of biomass burning from other regions. Consistently there is observed to be a variable start and end time changing year to year, starting as early as early august and ending as late as early November. Otherwise, this region tends to have very low levels of BC and generally is clean. This combination of conditions leads to it being an excellent candidate to represent long-range transport.

Beijing as a typical megacity, with a population more than 18 million, and considerable sources from high tech, industry, and government. Based on the total available three year's data in 2001, 2015 and 2016 the features in general appear to be like Taihu, consistent with the understanding that Beijing is also urban. The value of AOD during the highest period is about 3.2, while most of the second pass and third pass data fall in the range of 1.5~3, with the concept that the temporal occurrence of peak events is random but tending to be of similar magnitude. In addition, there is a considerable amount of the total data (37%) which behaves like long range transport. This tends to occur during spring, but only occuring in specific years (Han et al., 2015; Wang et al., 2015; Wang et al., 2004). This is consistent with the fact that transport from western china (Shanxi, Shaanxi, Ningxia, etc.) and its large amount of energy and downstream energy emissions sources, or northeastern china (and its heavy biomass burning and industrial emissions) does occur at times when spillover occurs over the mountains surrounding the edges of Hebei and Beijng (Li et al., 2022; Qin et al., 2022; Wang et al., 2020).

The temporal characteristics of AOD in the megacity of Hong Kong form another very interesting case, as observed in Figure 1(e). The value tends to have a relatively high mean with most measuremnts between 1.0 and 1.5, and seemingly occurring randomly throughout most of

the year. This result is consistent with its large industrial, transportation, and shipping sectors, and located in the middle of the highly populated and heavily industrialized Pearl River Delta region. However, there also is a recurring increase in the overall AOD (between 1.5 and 2.6) that occurs in October. These results are unexpected in Hong Kong when compared with many local studies (Tan et al., 2016; Fang et al., 2018; Xu et al., 2022), however they are consistent with recent studies which have focused on the changes in the Monsoon (Yang et al., 2006; Yao et al., 2008; Lau et al., 1997) and biomass burning increases throughout Northern Southeast Asia (Lin et al. 2020; Wang et al., 2021). A major difference is that these studies which have observed these changes are whole-atmospheric studies, not specifically related to measurements at the surface.

Lumbini in South Asia is a rapidly developing urban area in Nepal. The signal corresponds strongly with known urbanization, a high population density, and many small and randomized sources including rubbish and trash burning, small brick and cement kilns, and a growing proliferation of combustion-based transport options. The strength of the red signal varies in intensity and magnitude from an observed relative maximum in the middle and end of 2014 as development rapidly accellerated (Rupakheti et al., 2020).

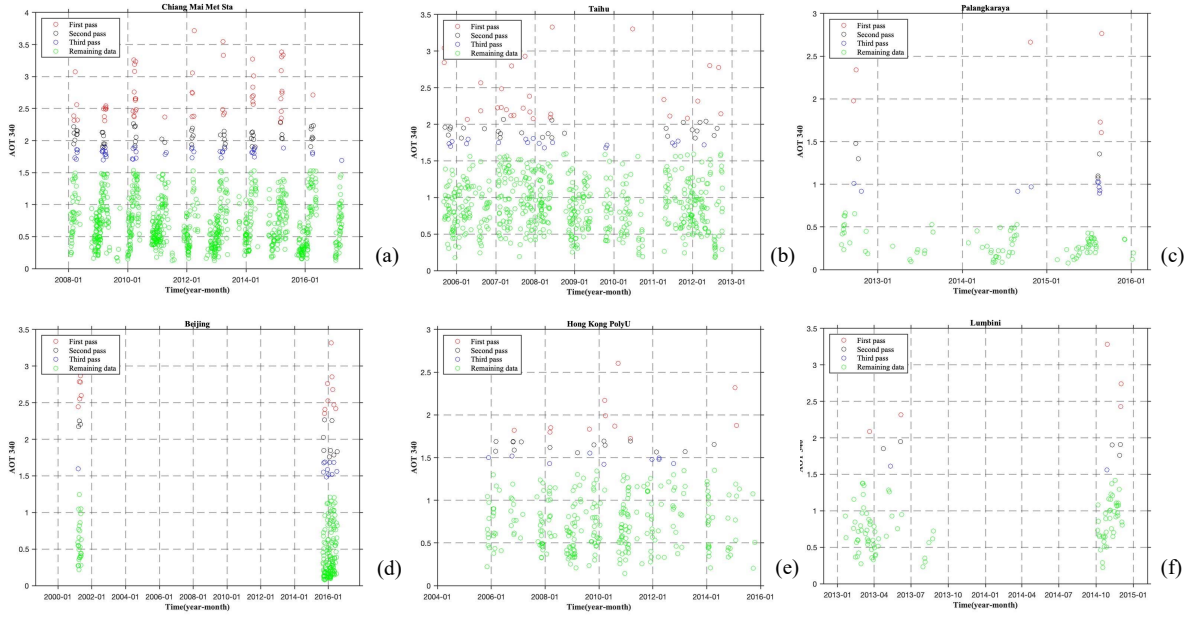

Figure 1. Time series of AOD at 340nm of different sites. (a) Chiang Mai Met Sta; (b) Taihu; (c) Palangkaraya; (d) Beijing; (e)Hong Kong PolyU; (f)Lumbini

3.2 Typical Features of Well-Defined Source Regions

To calculate the typical characteristics of biomass burning, the distribution of solutions of size pairs of core and shell radius corresponding to the intersection across all different wavebands of the measured SSA in Chiangmai during the high season will subsequently be used, hereafter called [BB], see Fig.2a. Since the burning in Chiangmai is local, the profile may be used to represent other regions which also have a significant local biomass burning source. If a region has a good match with the biomass profile, it implies that the local aerosol profile is influenced by local biomass burning. When a region has a good match with the biomass profile after being shifted upwards, it is consistent with a region that is impacted by biomass burning

which has undergone growth in-situ while undergoing transport between its source and where it was ultimately measured. In this case, an approximation of the age of the biomass burning can be obtained indirectly by considering how much upward shift is required to make the best fit, where the shift quantifies the amount of shell growth while in-situ.

Similarly, the distribution from Palangkaraya is useds to compute the conditions under which long-range transport occurs, subsequently called [LRT] (Wang et al., 2021), see Fig.2b. The AOD pattern of Palangkaraya shows a combination of relatively low mean and a high standard deviation of AOD, which starts and ends around the same time every year. Local measurements of CO from the long-term WMO station in the same city also has a similar signal (Aouizerats et al., 2014). Basically, the local environment is nearly pollution free, except for when biomass burning occurs on Sumatra, Borneo, and other islands in the region, which then transport to the site. For these reasons, measurements at this site are an excellent candidate to represent sites typically impacted by long-range transport.

Finally, the distribution of solutions of size pairs of core and shell radius corresponding to the measured SSA in Taihu referred to as [UR], see Fig.2c. Since Taihu is near the center of the world's largest conurbation, yet located in the middle of a lake, highways and other immediate point sources are reduced, making the profile highly representative of a generalized urban area.

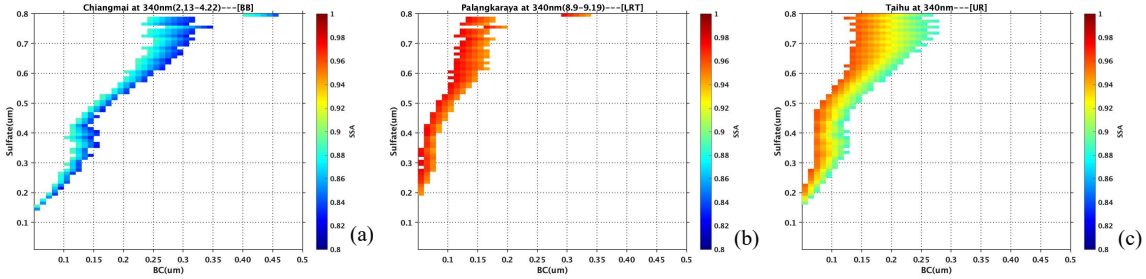

Figure 2. BC core and Sulfate shell size distributions, with corresponding SSA (color) at the three well-defined source sites: Chiangmai [BB], Palangkaraya [LRT], and Taihu [UR].

3.3 Quantifying New Spatial and Temporal Relationships in BC Properties Induced by Various Natural and Anthropogenic Forcings

The climatologically constrained SSA distribution in the 126 million population Greater Bay Conurbation (hereby defined based on measurements from the Hong Kong PolyU site) is given in Fig.3a. The climatological core and shell size distributions show mostly urban characteristics, as expected from the high population density, large and growing economic footprint in this region. However, the geographical location of Hong Kong places it in a region influenced by the Asian monsoon, in a dense urban area surrounded by significant agriculture, and upwind from the rapidly developing and transforming nations in ASEAN.

As expected, the overall climatology of aerosol properties in Hong Kong, based on the magnitude of the SSA (i.e., color) and size distribution of both the core and shell (i.e., shape of the SSA distribution) derived over this station is mostly dominated by [Urban], with very small amounts of [LRT] and [BB] (Fig 3a). However, both inter-annual and intra-annual variability are observed to be very important in this region.

A first case is observed in Fig 3b-c. Monsoon theory indicates that there is a strong Southeast wind occurring in July and August, leading to flow from the clean South China Sea to the Chinese Mainland, with Hong Kong being one of the first points of contact (Yang et al., 2014;

Lawrence and Lelieveld, 2010; Webster and Yang, 1992; Zhu et al., 2012). It has generally implied that during this time, the air should be extremely clean. And when analysis is done using all days from July and August as given in Fig 3b, the local signal is observed along with an LRT signal. However, a look at only the August data reveals a pure LRT signal (Fig.3c). Since the winds are not changing during this period of time, therefore the results are consistent with a significant change in the aerosol loading on the southern edge of the South China Sea. This is consistent with known massive fire events which occur starting in August on a nearly annual basis (Deng et al., 2021; Cohen, 2014; Cohen et al., 2017; Wang et al., 2020; Li et al., 2020; Chen et al., 2017). This data offers a first independent characterization of significant long range transport of biomass burning absorbing aerosol over 2000km from Borneo to Hong Kong.

Furthermore, it can be seen in Figs 3d-g that in 2006 the [Urban] source occupies the vast majority of the September/October/November signal, with a very small amount of BB mixed in, while the September/October/November signal in 2014 is found to mostly consist of LRT with only a small amount of Urban. Similarly, the January signals in 2014 and 2006 are also vastly different from each other, with 2014 being mostly Urban in nature, and 2006 having an extremely strong BB signal. All of these results are consistent with the fact that 2006 was a strong El-Nino and 2014 was a mixture of a budding La-Nina occurring at the same time as a negative IOD (Logan et al., 2008; Deng et al., 2021; Cohen, 2014; van der Werf et al., 2008; Rinsland et al., 2008; Chi et al., 2019; Xie and Fang, 2019).

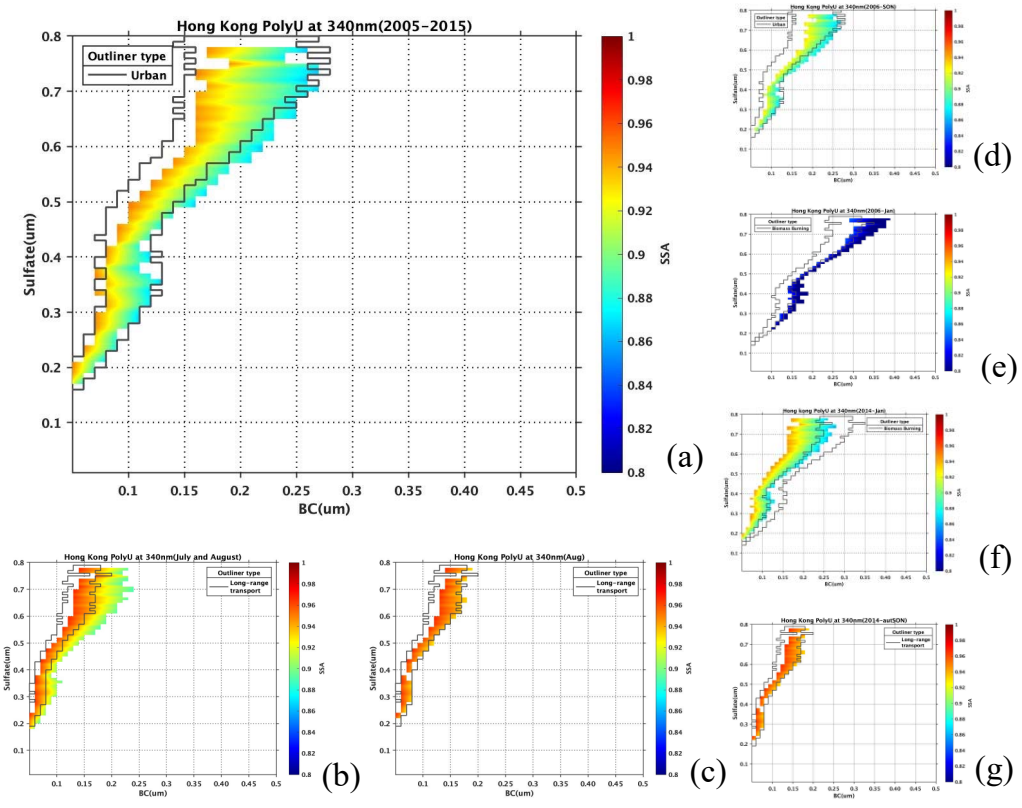

Figure 3. Constrained distribution of SSA from model result of Hong Kong PloyU during different special time periods with urban, Biomass Burning and Long-range transport profile.

Lumbini is located in Nepal and represents the densely populated Southern Slopes of the Himalayas, a region impacted by biomass burning, the Monsoon, and very large variance in aerosol loadings from ultra clean to some of the most polluted conditions on the planet. Fig 4 shows the constrained SSA distribution during three seasons where there are vastly different conditions observed.

First during the monsoon season (JJAS) the majority of the sources are influenced by long range transport, consistent with the squeezing of air from the Continent into the foothills of the Himalayas (Dumka et al., 2015; Rupakheti et al., 2017; Rupakheti et al., 2020; Chen et al., 2020). During this time, a mixture of long-range transport and urban aerosols are observed, with the solution covering a very wide range of particle radii from 210nm up to 1030nm. This result is consistent with the site being impacted by air masses both of a local origin as well as those having been transported very far away from regions with a very high loading. These results are consistent with the rapid onset in terms of wind speeds, and consistent direction from south to north. Localized fires, coupled with urban areas in Eastern India and Bangladesh are all upwind from Lumbini during this time. It is important to note that while heavy rain removes aerosols during this time of the year, that it also does not rain 24 hours a day 7 days a week over the entire domain, and therefore a significant amount of aerosols will be transported and not fully removed, consistent with findings by (Lee and Wang, 2015; Takeishi and Wang, 2021). This finding is further supported by the observed higher concentration of sulfate to BC ratio, requiring a smaller amount of overall freshly-emitted BC particles, and a longer time in-situ, both of which allow the surviving particles more time and greater opportunity to grow. It is also consistent with the highly humid atmosphere providing plenty of water to facilitate the growth of a shell. As demonstrated in Fig.4(a) the BC core size is less than 220nm, while the remaining 50 to 170nm is found in the shell.

Second, during the latter part of the cold season (Fig4c-d)(specifically JF) there is observed to be a large amount of locally dominated aerosol sources (both [Urban] and local [BB] associated with economic activity, solid fuel used for cooking, etc.), which in turn fit well with the observed types (Dumka et al., 2008; Kumar et al., 2015). However, during the earlier part of the cold season, also termed the harvest season (ND), the majority of the sources are influenced by local biomass burning, with the results showing that there is a very absorbing fraction of biomass burning type solely observed during this period of time (Rupakheti et al., 2017). The impact of crops being harvested and some straw being left to dry can be observed in both of these seasons, and is ultimately burned to clear the land, or stored and later burned for heating later in the winter, completely consistent with the observed mixture of [Urban] and [BB] profile match in JF (Engling et al., 2011; Lee and Wang, 2017; Duc et al., 2021). This result is further consistent with works by Rupakheti (2019) who demonstrated that aerosols during the post-monsoon season are mostly associated with the biomass burning. Wan et al (2017) who demonstrated the presence of biomass burning organic aerosol tracers is highest in winter and late autumn compared to other seasons of the year, and Liu and Cohen (2022) who demonstrated that areas in Northeastern India at the same time have a significant underestimate in NO_x emissions associated with biomass burning.

Overall, these conditions match well with the extensive use of local brick kilns and rubbish burning occurring in the winter, transport from India and Bangladesh during the monsoon, and burning of straw and other agricultural waste during the harvest season. However, given that the cold period has 2 different phases, further work should be clear about which of the two phases is being indicated when analyzing the impacts of biomass burning in this part of the world.

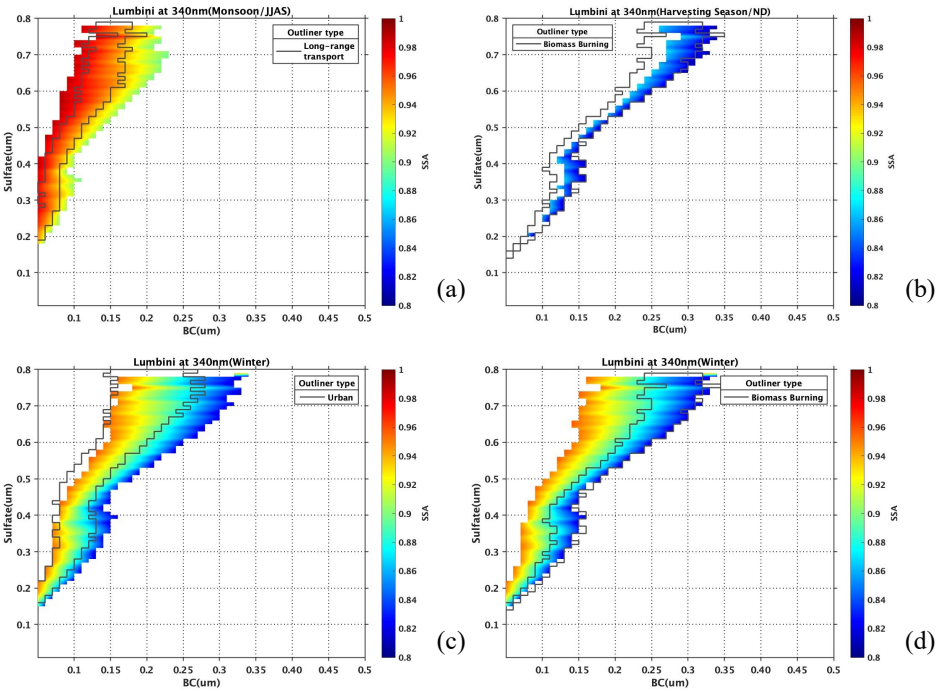

Figure 4. Constrained distribution of SSA from model result of Lumbini during winter(DJF), Harvest season and Monsoon with urban, Biomass Burning and Long-range transport profile.

Beijing is a highly dense urban area with a very large population, extensive private transport and without much heavy industry, indicating that an urban profile would generally be expected to dominate. Figure 5 demonstrates that over 9 months of the year, that there is a very strong urban signal in the data, when analyzed on a month-by-month basis. However, Beijing is also located at the foothills of mountainous regions to the West and North, and therefore can be subject to biomass burning and dust transport due to its unique geography.

A deeper investigation of the month-by-month properties show a clear intra-annual pattern which coherently and smoothly changes on a month-by-month basis, transitioning from one aerosol type to another, a very different finding from the hundreds of studies grouping Beijing aerosol properties on a seasonal basis (Liu et al., 2019; Wang et al., 2016; Han et al., 2014; Sun et al., 2015; Hu et al., 2017; Zhang et al., 2013; Zheng et al., 2005). November and December demonstrate a strong, narrow, and pure [BB] signal, while January has a strong [BB] signal, but one which is slightly less narrow. Feburary continues this transition to smaller BC core sizes and higher SSA values, with the entire pattern from January shifted to the left by 0.03um, demonstrating a mix of both [BB] and [Urban] signals. March continues this leftward shift and thickening of the solution space, with nearly all of the results falling in the [Urban] range, while also comprehensively filling the breadth of the [Urban] signal. Both April and May reveal a pure [Urban] signal, without [BB] or [LRT] being observed. This is also observed in September, but in this case, it is transitioning in terms of larger BC cores in the opposite direction from [LRT] back towards [BB]. In June, the signal shifts further left, with a loss of some [Urban] signal and a growing signal of [LRT]. In July, the maximum [LRT] contribution is obtained, with the [LRT] contributing roughly 50% and the [Urban] contributing the remainder. August starts to shift in the opposite direction, with the BC core size growing, and the fraction of [LRT] decreasing to 40% and the fraction of [Urban] increasing. Finally, in October, the signal is thinner on average

and consists of mostly [Urban] signal and a small amount of [BB]. These results are indicative of the fact that while Beijing is an urban area, and the measurement site is located in the northern part of the urban core, that the sources of aerosols are highly variable from month-to-month, including biomass burning from near-by, and long-range-transported sources from beyond the JingJinJi area. It is hoped that further projects analyzing sources and profiles of absorbing aerosols in Beijing will look at a higher time frequency and move beyond the season-to-season approach currently adapted by the community. Some specific examples are that the biomass burning seems to cut between both the late Autumn and early Winter periods, and that the large sources of long-range transport seem to mostly exist in early summer, but over a shorter period than the summer as a whole. The fact that each month except for November and December is unique, indicates that there are far more complex forces at work.

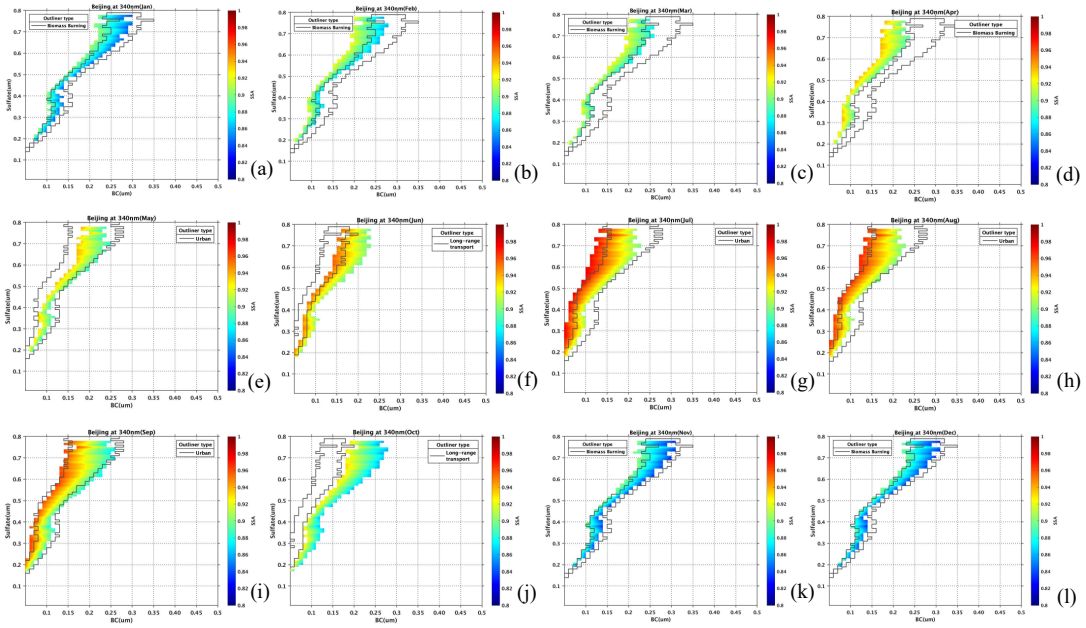

Figure 5. Constrained distribution of SSA month-by-month, demonstrating Urban, BB, LRT profiles all during different times of the year.

The resulting BC and shell size information during only the high periods of AOD in time (as displayed in Fig.1) are shown in Fig.6. This focus on when the AOD is highest offers the perspective of the properties of the BC and shell size when the loadings are most significant. There is a clear long range transport path observed at both Dongsha Island and Chen Kung University, and a very small probability of long-range transport identified in Hong Kong, all of which are consistent with the high biomass burning time periods found throughout Continental Southeast Asia (Lin et al., 2014; Chan et al., 2003; Lee et al., 2017; Sahu et al., 2014). These results are found to match very well with the standard [LRT] signal observed in Chiangmai, but shifted vertically upwards. This result is consistent with the source being biomass burning from Chiangmai and other surrounding areas (Huang et al., 2013; Fu et al., 2012; Chuang et al., 2015), which later transports to Dongsha and Chen Kung. While in-route, there is continued in-situ growth due to SO_2, NO_2, and VOCs from urban areas, and DMS from the South China Sea. The high time first appears in Hong kong from February 12 through April 13, with only 2% of the total solution being [LRT], which given the local magnitude of emissions during the dry season

in the GBA area (Chen et al., 2020; Duc et al., 2021), may still offer a somewhat significant impact. The contribution in Dongsha is observed from February 19 to April 22 with a far larger percentage of of [LRT] at 42%, due to the fact that Dongsha does not have local sources (except for shipping), but it is still close enough to the GBA that it may contain some not-so-aged transported aerosols. Finally, the contribution in Chen Kung is observed from March 3 to May 8 and has 62% of [LRT], indicating that long range transport dominates the total loading there, consistent with the fact that there are very few local sources.

Under the assumption that Chiangmai is the source of the biomass burning, the particles will travel from west to east, first arriving in Hong Kong, next arriving at Dongsha, and finally at Chen Kung, assuming that the eastern wind in the lower free troposphere is relatively steady (Wang et al., 2013; Liu et al., 1999). Various one-off experiments and model studies have been conducted to study the impacts of the annually varying biomass burning events occurring in Continental Southeast Asia on surrounding areas. While there are many such studies which have demonstrated the plume in the near-downwind areas including Vietnam, Guangxi and Hainan (Huang et al., 2020; Ding et al., 2004; Li et al., 2007; Ding et al., 2021; Ding et al., 2013), there are very few which have been able to successfully transport as far as we have observed here (Cohen, 2014; Wang et al., 2021). Furthermore, while modeling studies of individual single fire events transporting in such a manner have been found (Aouizerats et al., 2015; Yen et al., 2013; Cohen et al., 2017; Wang et al., 2021), there has been no clear observational study, using data over multiple years (12 at Chen Kung, 10 at Hong Kong, and 6 at Dongsha), in which such a finding has been made. Furthermore, these findings are not limited in time to a single season or a single transport event, and provide a comprehensive, fully measurement based analysis.

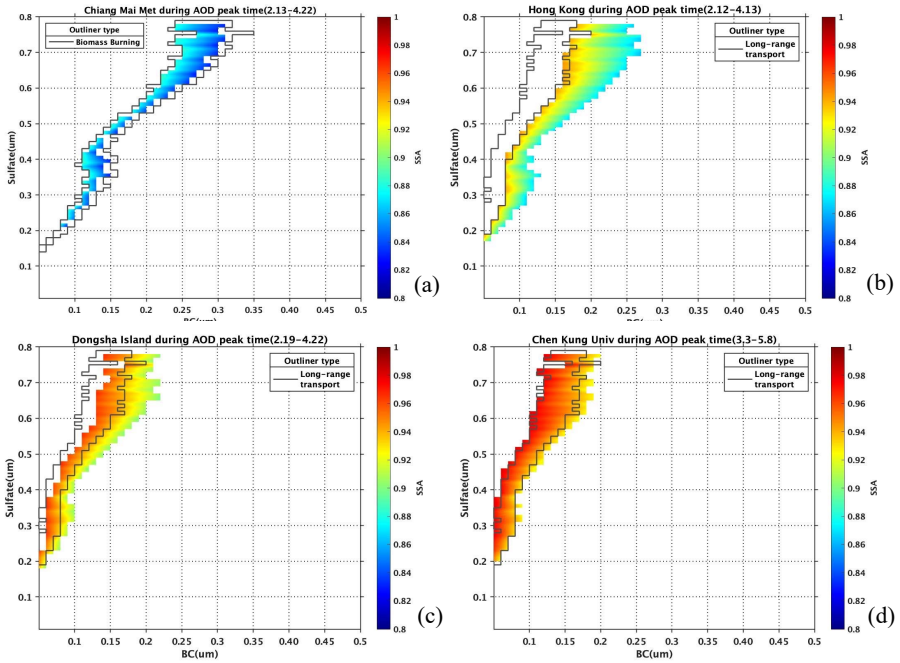

Figure 6. Constrained distribution of SSA from model result of sites that located along possible transport path.

4 Applications of Results

4.1 In-situ Lifetime of Sulfur Dioxide

The computed e-folding time is generally long, consistent with the fact that the air parcels have spent a significant amount of time being transported through the free troposphere, as demonstrated in Table 1. These e-folding times are approximated around the idea of DMS and/or anthropogenic SO_2 decaying into SO^{4-} which then condenses onto the shell. The results are not strongly influenced by the quick removal of SO_2 and conversion into H_2SO_4 that occurs in the boundary layer near emissions sources under very high OH, wet and warm conditions found in heavily polluted conditions in this part of the world. Instead, the aging is mainly controlled by gas phase oxidation process happening in cooler and lower pressure air, which is also more likely to be exposed to UV radiation since it is found above the cloud layer. The results therefore should be consistent with relatively higher amounts of OH (closer to urban than background), due in part to the extra amount of UV radiation available above the cloud layer. Additionally, the results should show slower growth due to the lower pressure and cooler conditions. Base on equation (3) the maximum and minimum lifetime of SO_2 in two different chemical background conditions (the background case results are given in the columns of 4 and 5; the urban case results are given in the columns of 6 and 7) are calculated in this manner and listed in Table 1 and the possible uncertainty have been evaluated.

The results are consistent with the lifetime of SO_2 being longer as compared to the lifetime in the boundary layer where the temperature and recycling of OH are both high. In the free troposphere, although the OH may be high due to stronger UV, the lack of water vapor and VOCs lead to OH regeneration being very slow. Since the lifetime in urban areas is faster, it would make sense that by efficiently reducing the SO_2 emitted from urban areas, the longer timescale the aging of BC and sulfate is reduced (Cohen et al., 2011) for the BC emitted from the biomass burning and subsequently transported downwind over urban areas. Overall, while these lifetimes are long, they are not so long as to be ruled out based on the amount of time it takes to transport form the source region to the measured destination.

Testing the values of the e-folding time under background OH conditions yield a maximum lifetime with a value ranging from 21 to 32 days and a minimum ranging from 16 to 20 days. This increase in the amount of time, in particular for the minimum number of days from 10 to 16 leads to a set of solutions which are likely not possible. The amount of time required to grow would be more than the amount of time that it would take to be transported. Overall, the breadth of the solution range for lifetime is different between the minimum and maximum cases, consistent with the fact that the decay of atmospheric SO_2 into sulfate is slower than expected, but still reasonable in the case of a higher OH concentration, with the difference from 0 days to 9 days. The results require that a significant amount of the total BC is observed above the boundary layer.

There are other possible methods and assumptions which could be made to decrease the aging lifetime, which have not been considered herein due to the lack of data. First, higher levels of SO_2 that provided by CAMS, possibly due to increased vertical transport of SO_2 from urban areas along the path of transport, or from heightened DMS emissions or from faster chemical processing of DMS could lead to higher M(env.) in equation 3. Second, this work didn't consider the NO_2+OH reaction to calculate HNO_3, which is optically the same as H_2SO_4 and has the same effect on the result, which will make the in-situ lifetime shorter. Third, this work didn't consider reactions which may occur on the liquid water existing on the coated BC surface (e.g. potentially

555 sulfate aerosol production via aqueous phase oxidation), which would also make the in-situ
556 lifetime shorter. If all these processes are taken into consideration, it would make the in-situ
557 lifetime shorter, but not so short that the background OH cases would then be too short to match
558 with the transport lifetimes. In general, the difference between the max lifetime of background
559 OH and the min lifetime of urban OH allow the real world observed transport lifetime to be
560 matched, based on the assumption of whether the oxidation and growth is purely based on the
561 gas-phase oxidation and equation 1, or whether these other processes are also important.

Site_name	Longitude	Latitude	Max(BG,days)	Min(BG,days)	Max(UR,days)	Min(UR,days)
ARM_Darwin	130.891	-12.425	27	25	17	15
ARM_Nainital	79.458	29.359	23	19	15	12
Anmyon	126.33	36.539	25	19	16	13
Bac_Giang	106.225	21.291	26	20	17	12
Bac_Lieu	105.73	9.28	22	16	14	10
Baengnyeong	124.63	37.966	28	22	17	14
Bandung	107.61	-6.888	26	21	16	13
Beijing	116.381	39.977	30	26	21	17
Beijing-CAMS	116.317	39.933	28	24	18	15
Chen-Kung_Univ	120.217	23	24	18	15	12
Chiang_Mai_Met_Sta	98.972	18.771	—	—	—	—
Chiayi	120.496	23.496	26	20	16	13
Darwin	130.892	-12.424	—	—	—	—
Dhaka_University	90.398	23.728	29	24	19	15
Doi_Ang_Khang	99.045	19.932	29	23	19	14
Dongsha_Island	116.729	20.699	23	17	14	11
EPA-NCU	121.185	24.968	26	21	17	13
Fukuoka	130.475	33.524	30	21	19	13
Gandhi_College	84.128	25.871	31	23	19	14
Gangneung_WNU	128.867	37.771	26	20	16	12
Gosan_SNU	126.162	33.292	21	18	13	12
Gual_Pahari	77.15	28.426	31	25	20	15
Gwangju_GIST	126.843	35.228	26	20	16	12
Hankuk_UFS	127.266	37.339	29	22	18	14
Hokkaido_University	141.341	43.075	26	21	16	13
Hong_Kong_PolyU	114.18	22.303	31	22	19	14
Jabiru	132.893	-12.661	27	23	17	14
Jaipur	75.806	26.906	28	21	18	13
Jomsom	83.714	28.778	25	21	16	13
KORUS_Kyungpook_NU	128.606	35.89	26	21	16	13
KORUS_UNIST_Ulsan	129.19	35.582	25	22	15	14
Kaashidhoo	73.466	4.965	26	19	16	12

Kanpur	80.232	26.513	31	24	19	15
Kathmandu-Bode	85.39	27.68	—	—	—	—
Kathmandu_Univ	85.538	27.601	31	26	19	16
Lahore	74.325	31.542	31	22	19	14
Luang_Namtha	101.416	20.931	30	23	16	14
Lumbini	83.28	27.49	—	—	—	—
Mukdahan	104.676	16.607	26	19	16	12
NCU_Taiwan	121.192	24.967	26	21	17	13
NGHIA_DO	105.8	21.048	27	20	17	13
Nainital	79.458	29.359	28	22	18	14
Nong_Khai	102.717	17.877	29	21	18	13
Noto	137.137	37.334	26	19	16	12
Osaka	135.591	34.651	24	20	15	12
Palangkaraya	113.946	-2.228	—	—	—	—
Pimai	102.564	15.182	26	20	16	12
Pokhara	83.971	28.151	27	26	17	16
Pune	73.805	18.537	31	27	20	17
Pusan_NU	129.083	35.235	28	21	17	13
SACOL	104.137	35.946	32	26	20	16
Seoul_SNU	126.951	37.458	28	21	18	13
Shirahama	135.357	33.693	24	18	15	11
Silpakorn_Univ	100.041	13.819	29	21	18	13
Singapore	103.78	1.298	23	18	15	11
Son_La	103.905	21.332	30	20	19	13
Songkhla_Met_Sta	100.605	7.184	24	17	15	11
Taihu	120.215	31.421	—	—	—	—
Taipei_CWB	121.5	25.03	26	21	17	13
Taiping	114.362	10.376	—	—	—	—
USM_Penang	100.302	5.358	23	17	14	11
Ubon_Ratchathani	104.871	15.246	25	18	16	11
Ussuriysk	132.163	43.7	30	23	19	15
Vientiane	102.57	17.992	26	20	17	12
XiangHe	116.962	39.754	30	23	19	14
Xinglong	117.578	40.396	30	22	19	14
Yonsei_University	126.935	37.564	24	22	15	14
Yulin	109.717	38.283	30	29	19	18

562

4.2 Sensitivity of Solutions to Different AERONET Data Assumptions

The AERONET measurements contain some data which is of lower or questionable quality as compared to the bulk of the data. This is frequently due to either not enough absorption to successfully measure the SSA (i.e., when the AOD<0.4), non-successfully cleared thin clouds, or other such phenomenon. To account for this uncertainty, this work has previously focused solely on the middle 80% of the total SSA measurements for each given dataset at each wavelength and time period studied. By discarding the top and bottom 10%, the reliability of the remaining measurements is much higher, and therefore the model results are more believable. The fact that differences on a monthly-basis are already clearly observed is proof that this is a reasonable approach.

However, selecting the central 80% is also arbitrary. So, a further sensitivity study is done to consider the effects of choosing the central 90% and 70% of data respectively, and quantify the impact of this cutoff on the computed BC and SO_4 size distributions. The results are given in Fig.7. A respective use of 70% and 90% of the data lead to a slightly biased change, although not leading a significant overall difference. In the case of 70% of data, the SSA distribution reduces by 32%, 27% and 30% respectively in the urban, LRT and BB cases. As observed, there is a slight bias with the decrease in urban being a further separation from LRT, and the decrease in BB being a move towards urban. In the case of 90% of data, the SSA distribution increases by 23%, 25.7% and 50% respectively in the urban, LRT and BB cases. As observed, there is a slight bias in the LRT case, in which case it extends further from the urban and in the BB case, in which case it also extends further from the urban. However, in all cases, the biases do not significantly alter the shape, and if anything, make it easier to distinguish the different underlying factors from each other.

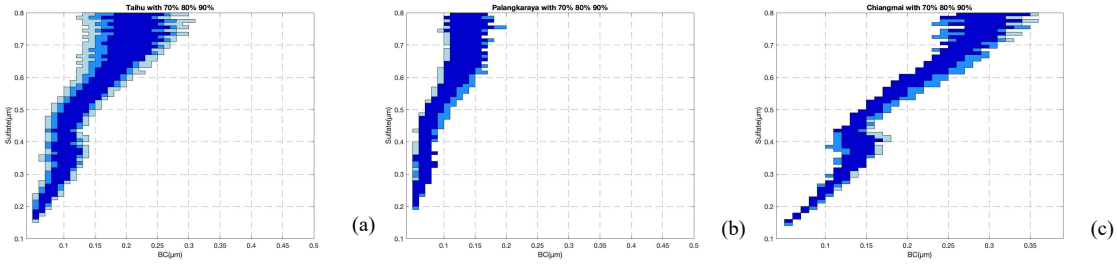

Figure.7 SSA distribution of three profiles with different amount of AERONET measurement data used to constrain the MIE inversion. When the central 70% of the measurements are used, the results are given in dark blue, when the standard 80% of the measurements are used the results are given in medium blue, and when the central 90% of the measurements are used the results are given in light blue. The plot on the left is for Urban, the plot in the center is for LRT, and the plot on the right is for BB.

4.3 Comparison with Independent Measurements

The MIE model inverted core and shell sizes in Beijing overlap at the same time with measurements taken by SP2 in Beijing from 2016.11.10 to 2017.01.12, as shown in Fig.8a. The inverted ratio of Dp/Dc from the MIE model approach and as observed from SP2 are shown in Fig.8b. This comparison assumes that the refractive index of core and shell are the same between the surface SP2 measurements and the column inverted Mie outputs. In general, the two methods

compare well with each other, with nearly all of the SP2 measurements (the 99.5% larger than 1.2) falling within the range of the MIE model inverted results. Next, the bulk of the SP2 data occurs with a ratio of 1.4-1.6, which also happens to be the mode of the range of outputs of the MIE model inversion. The only discrepancy is that the MIE model inversion has a range of values with Dp/Dc larger than 2, which is not observed in the SP2 data.

There are a few known possibilities for this discrepancy. First, is that the SP2 may fail to capture very small particles of BC, which may disaggregate or disintegrate when being hit by the laser associated with the SP2 detector. Similarly, some of the sulfate shell may be evaporated due to the heating of the BC, leading to a smaller than actual shell being measured. A third possible source of disagreement is that the SP2 only measures particles near the ground, while AERONET measures particles throughout the troposphere, and particles which are aloft as pointed out already, are more likely to have been in the air longer, and therefore be more significantly aged, leading to a larger value of Dp/Dc. It is possible that the ageing scale or transport range observed at the surface urban site may not pick up the fact that there are some biomass burning aerosols which are mixed into the total column but not necessarily at the surface, consistent with the fact that 28% of the observed solution space is BB while 72% is Urban.

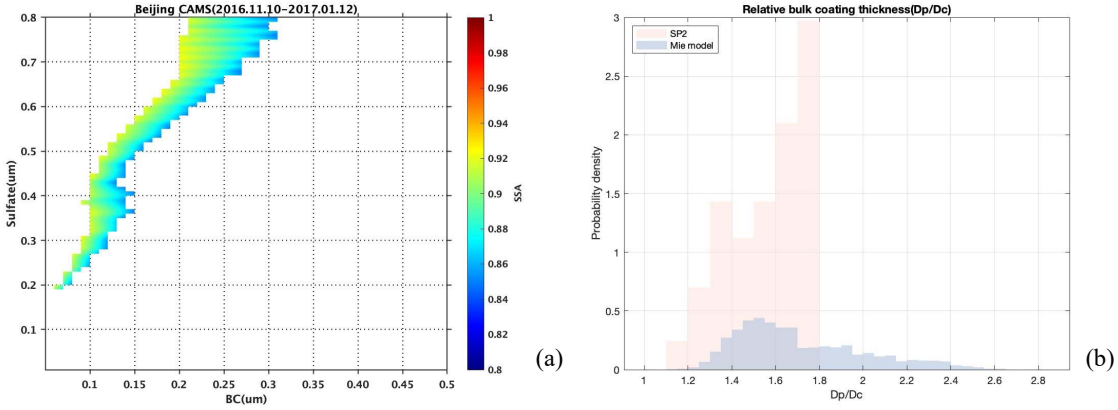

Figure.8 Size distribution during overlapping time period between AERONET and SP2 measurement in Beijing(left) plot. Probability density comparison of Dc and Dp/Dc of two datasets.

5 Conclusions

Applying a Mie-model with a core-shell approximation over multiple UV bands of the observed clear sky AERONET SSA has successfully allowed for a new inversion of BC and shell size and mixing state information to be obtained. These results are observed to group very well at typical geographical locations with well characterized BC properties. These results help deepen the understanding of first order chemical aging and particulate growth, and how the distribution of particle size and absorbing optical characteristics behave under these different classifications. By narrowly focusing on the size of BC, the size of the refractive shell, and the mixing state, results are found to be consistent with advanced modeling studies and independent measurements. The results conform very well over regions that are known to be heavily polluted, both in terms of urban, biomass burning, long-range transport and mixed sources.

Deeper analysis of the temporal and spatial variance, allows for disentanglement of overlapping source types, clearly identifing multiple characteristics as a function of space and time. Some of these characteristics are mixed in time with others, showing that multiple source types are possible to quantify in a probabilistic manner. These results are consistent with the atmospheric column quite reasonablying having different sources located near the surface from those observed at the same time in the free troposphere. During specific times, individual sites are observed to rapidly transition from one dominant characteristic state to a different one, indicating significant different sources, atmospheric properties, and driving factors behind the aerosol distribution, even within a single geographic place. Frequently these changes occur at time scales with short temporal duration, although consistently across many different years, indicating new definitions of climate, season, and dynamical driving patterns may be more appropriate to use, rather than standard climatological definitions.

The work demonstrates that these types can be successfully divided into three distinct and unique size distributions for [Urban], [BB] and [LRT] conditions. These findings are applied across many different regions in terms of geography, economic development levels, and national boundaries, all of which have their own unique air pollution control rules, environmental goals, and air pollution emissions characterizations. Three excellent examples are observed in Hong Kong, Kathmandu and Beijing. These sites clearly exhibit local sources as expected, but also have periods of time where intense biomass burning, long range transport, and mixtures of these dominate. However, such shifts frequently occur only during specific months, although these patterns are found to hold consistently over many years. In each case, there is an unexpected scientific result: Hong Kong is found to have long-range transport during the Asian Monsoon (usually thought to be clean), associated with LRT transport from Southeast Asia; Nepal is found to have LRT during the monsoon rapidly switching to BB post Asian Monsoon, even when the region experiences the Monsoon rains; and Beijing is exhibited to have all different types slowing shifting from one to another and back, but only observed on a month-by-month basis, vastly different from the typical analyses which group Beijing season-by-season and do not identify these regular occuring and shifting patterns.

Based on how these best fit distributions change in time, in specific being shifted from a standard distribution to one with more shell growth, allows for an indirect way to quantify in-situ lifetime. This is clearly observed across many of the sites, allowing for a new observational constraint on the lifetime of aerosols and a quantitative way to constrain the mixing between local and non-local sources. The in-situ age of aerosols at different sites reveals a vast difference in in-situ lifetime, ranging from a week and a half up to a month, based on assumptions of the time of year and pure gas-phase aging and growth. Since these changes are observed throughout the total column, they are reflective of lifetime on a climatological scale, and provide support to many studies which have indicated that absorbing aerosols can transport significant distances, such as across the Pacific Ocean and to the three poles.

This work demonstrates that control strategies can be strategically developed for each individual location and adapted during different times of the year. Locations which have a single type would adopt a single stragey, while those with multiple times or time varying types would develop strategies which are multi-perspective and vary from time to time. This approach may allow for significant cost savings and/or more efficient control efforts. Locations with special events could opt for control of different types and amounts during different periods of the year. This flexibility will provide new opportunities to enhance the local atmospheric environment.

Acknowledgments

This work is supported by the National Natural Science Foundation of China (42075147) and the China University of Mining and Technology Scientific Research Platforms Construction Fund (102521185). This work thanks the PIs of the AERONET, CAMS for making their data available.

Author contributions

The first draft of the review was prepared by **Xinying Wang**: Conceptualization, Writing - original draft, Data curation, Writing - review & editing, Investigation, Formal analysis, Software. **Jason Blake Cohen**: Conceptualization, Data curation, Writing - original draft, Writing - review & editing, Formal analysis, Funding Acquisition, Supervision**. Shuo Wang** software and visualization.

Data Availability Statement

The AERONET datasets used in this study are available at https://aeronet.gsfc.nasa.gov/new_web/data_description_AOD_V2.html . The CAMS global reanalysis product EAC4 is available at https://ads.atmosphere.copernicus.eu/cdsapp#!/dataset/cams-global-reanalysis-eac4-monthly?tab=overview . The SP2 measurements in Beijing are available at https://data.ceda.ac.uk/badc/aphh/data/beijing/man-sp2. All of the data and underlying figures are available for download at https://figshare.com/s/a8a98c6dbb7d7b50dabc.

References

An, J., Huang, Y., Huang, C., Wang, X., Yan, R., Wang, Q., Wang, H., Jing, S., Zhang, Y., Liu, Y., Chen, Y., Xu, C., Qiao, L., Zhou, M., Zhu, S., Hu, Q., Lu, J., & Chen, C. (2021). Emission inventory of air pollutants and chemical speciation for specific anthropogenic sources based on local measurements in the Yangtze River Delta region, China. In Atmospheric Chemistry and Physics (Vol. 21, Issue 3, pp. 2003–2025). Copernicus GmbH. https://doi.org/10.5194/acp-21-2003-2021

Aouizerats, B., Thouron, O., Tulet, P., Mallet, M., Gomes, L., & Henzing, J. S. (2010). Development of an online radiative module for the computation of aerosol optical properties in 3-D atmospheric models: validation during the EUCAARI campaign. In Geoscientific Model Development (Vol. 3, Issue 2, pp. 553–564). Copernicus GmbH. https://doi.org/10.5194/gmd-3-553-2010

Aouizerats, B., van der Werf, G. R., Balasubramanian, R., & Betha, R. (2015). Importance of transboundary transport of biomass burning emissions to regional air quality in Southeast Asia during a high fire event. In Atmospheric Chemistry and Physics (Vol. 15, Issue 1, pp. 363–373). Copernicus GmbH. https://doi.org/10.5194/acp-15-363-2015

Bohren, C. F., & Huffman, D. R. (1998). Absorption and Scattering of Light by Small Particles. Wiley. https://doi.org/10.1002/9783527618156

Bollasina, M. A., Ming, Y., Ramaswamy, V., Schwarzkopf, M. D., & Naik, V. (2014). Contribution of local and remote anthropogenic aerosols to the twentieth century weakening of the South Asian Monsoon. In Geophysical Research Letters (Vol. 41, Issue 2, pp. 680–687). American Geophysical Union (AGU). https://doi.org/10.1002/2013gl058183

Bond, T. C. (2001). Spectral dependence of visible light absorption by carbonaceous particles emitted from coal combustion. In Geophysical Research Letters (Vol. 28, Issue 21, pp. 4075–4078). American Geophysical Union (AGU). https://doi.org/10.1029/2001gl013652

Bond, T. C., & Bergstrom, R. W. (2006). Light Absorption by Carbonaceous Particles: An Investigative Review. In Aerosol Science and Technology (Vol. 40, Issue 1, pp. 27–67). Informa UK Limited. https://doi.org/10.1080/02786820500421521

Bond, T. C., Doherty, S. J., Fahey, D. W., Forster, P. M., Berntsen, T., DeAngelo, B. J., Flanner, M. G., Ghan, S., Kärcher, B., Koch, D., Kinne, S., Kondo, Y., Quinn, P. K., Sarofim, M. C., Schultz, M. G., Schulz, M.,

Venkataraman, C., Zhang, H., Zhang, S., … Zender, C. S. (2013). Bounding the role of black carbon in the climate system: A scientific assessment. In Journal of Geophysical Research: Atmospheres (Vol. 118, Issue 11, pp. 5380–5552). American Geophysical Union (AGU). https://doi.org/10.1002/jgrd.50171

Chan, C. Y. (2003). Characteristics of biomass burning emission sources, transport, and chemical speciation in enhanced springtime tropospheric ozone profile over Hong Kong. In Journal of Geophysical Research (Vol. 108, Issue D1). American Geophysical Union (AGU). https://doi.org/10.1029/2001jd001555

Chen, Q.-X., Huang, C.-L., Yuan, Y., Mao, Q.-J., & Tan, H.-P. (2020). Spatiotemporal Distribution of Major Aerosol Types over China Based on MODIS Products between 2008 and 2017. In Atmosphere (Vol. 11, Issue 7, p. 703). MDPI AG. https://doi.org/10.3390/atmos11070703

Chen, Y., Morton, D. C., Andela, N., van der Werf, G. R., Giglio, L., & Randerson, J. T. (2017). A pan-tropical cascade of fire driven by El Niño/Southern Oscillation. In Nature Climate Change (Vol. 7, Issue 12, pp. 906–911). Springer Science and Business Media LLC. https://doi.org/10.1038/s41558-017-0014-8

Chen, Y., Yan, H., Yao, Y., Zeng, C., Gao, P., Zhuang, L., Fan, L., & Ye, D. (2020). Relationships of ozone formation sensitivity with precursors emissions, meteorology and land use types, in Guangdong-Hong Kong-Macao Greater Bay Area, China. In Journal of Environmental Sciences (Vol. 94, pp. 1–13). Elsevier BV. https://doi.org/10.1016/j.jes.2020.04.005

Cheng, Y. F., Wiedensohler, A., Eichler, H., Su, H., Gnauk, T., Brüggemann, E., Herrmann, H., Heintzenberg, J., Slanina, J., & Tuch, T. (2008). Aerosol optical properties and related chemical apportionment at Xinken in Pearl River Delta of China. In Atmospheric Environment (Vol. 42, Issue 25, pp. 6351–6372). Elsevier BV. https://doi.org/10.1016/j.atmosenv.2008.02.034

Chi, J., Du, Y., Zhang, Y., Nie, X., Shi, P., & Qu, T. (2019). A new perspective of the 2014/15 failed El Niño as seen from ocean salinity. In Scientific Reports (Vol. 9, Issue 1). Springer Science and Business Media LLC. https://doi.org/10.1038/s41598-019-38743-z

Chin, M., Jacob, D. J., Gardner, G. M., Foreman-Fowler, M. S., Spiro, P. A., & Savoie, D. L. (1996). A global three-dimensional model of tropospheric sulfate. In Journal of Geophysical Research: Atmospheres (Vol. 101, Issue D13, pp. 18667–18690). American Geophysical Union (AGU). https://doi.org/10.1029/96jd01221

Chuang, C. C., Penner, J. E., Taylor, K. E., Grossman, A. S., & Walton, J. J. (1997). An assessment of the radiative effects of anthropogenic sulfate. In Journal of Geophysical Research: Atmospheres (Vol. 102, Issue D3, pp. 3761–3778). American Geophysical Union (AGU). https://doi.org/10.1029/96jd03087

Chuang, M.-T., Fu, J. S., Lin, N.-H., Lee, C.-T., Gao, Y., Wang, S.-H., Sheu, G.-R., Hsiao, T.-C., Wang, J.-L., Yen, M.-C., Lin, T.-H., Thongboonchoo, N., & Chen, W.-C. (2015). Simulating the transport and chemical evolution of biomass burning pollutants originating from Southeast Asia during 7-SEAS/2010 Dongsha experiment. In Atmospheric Environment (Vol. 112, pp. 294–305). Elsevier BV. https://doi.org/10.1016/j.atmosenv.2015.04.055

Cohen, J. B. (2014). Quantifying the occurrence and magnitude of the Southeast Asian fire climatology. In Environmental Research Letters (Vol. 9, Issue 11, p. 114018). IOP Publishing. https://doi.org/10.1088/1748-9326/9/11/114018

Cohen, J. B., & Wang, C. (2014). Estimating global black carbon emissions using a top-down Kalman Filter approach. In Journal of Geophysical Research: Atmospheres (Vol. 119, Issue 1, pp. 307–323). American Geophysical Union (AGU). https://doi.org/10.1002/2013jd019912

Cohen, J. B., Lecoeur, E., & Hui Loong Ng, D. (2017). Decadal-scale relationship between measurements of aerosols, land-use change, and fire over Southeast Asia. In Atmospheric Chemistry and Physics (Vol. 17, Issue 1, pp. 721–743). Copernicus GmbH. https://doi.org/10.5194/acp-17-721-2017

Cohen, J. B., Prinn, R. G., & Wang, C. (2011). The impact of detailed urban-scale processing on the composition, distribution, and radiative forcing of anthropogenic aerosols. In Geophysical Research Letters (Vol. 38, Issue 10, p. n/a-n/a). American Geophysical Union (AGU). https://doi.org/10.1029/2011gl047417

Cooke, W. F. (2002). A general circulation model study of the global carbonaceous aerosol distribution. In Journal of Geophysical Research (Vol. 107, Issue D16). American Geophysical Union (AGU). https://doi.org/10.1029/2001jd001274

Cooke, W. F., Liousse, C., Cachier, H., & Feichter, J. (1999). Construction of a 1° × 1° fossil fuel emission data set for carbonaceous aerosol and implementation and radiative impact in the ECHAM4 model. In Journal of Geophysical Research: Atmospheres (Vol. 104, Issue D18, pp. 22137–22162). American Geophysical Union (AGU). https://doi.org/10.1029/1999jd900187

Corrigan, C. E., Ramanathan, V., & Schauer, J. J. (2006). Impact of monsoon transitions on the physical and optical properties of aerosols. In Journal of Geophysical Research (Vol. 111, Issue D18). American Geophysical Union (AGU). https://doi.org/10.1029/2005jd006370

Croft, B., Pierce, J. R., & Martin, R. V. (2014). Interpreting aerosol lifetimes using the GEOS-Chem model and constraints from radionuclide measurements. In Atmospheric Chemistry and Physics (Vol. 14, Issue 8, pp. 4313–4325). Copernicus GmbH. https://doi.org/10.5194/acp-14-4313-2014

Deng, W., Cohen, J. B., Wang, S., & Lin, C. (2021). Improving the understanding between climate variability and observed extremes of global NO2 over the past 15 years. In Environmental Research Letters (Vol. 16, Issue 5, p. 054020). IOP Publishing. https://doi.org/10.1088/1748-9326/abd502

Ding, A., Wang, T., & Fu, C. (2013). Transport characteristics and origins of carbon monoxide and ozone in Hong Kong, South China. In Journal of Geophysical Research: Atmospheres (Vol. 118, Issue 16, pp. 9475–9488). American Geophysical Union (AGU). https://doi.org/10.1002/jgrd.50714

Ding, A., Wang, T., Zhao, M., Wang, T., & Li, Z. (2004). Simulation of sea-land breezes and a discussion of their implications on the transport of air pollution during a multi-day ozone episode in the Pearl River Delta of China. In Atmospheric Environment (Vol. 38, Issue 39, pp. 6737–6750). Elsevier BV. https://doi.org/10.1016/j.atmosenv.2004.09.017

Ding, K., Huang, X., Ding, A., Wang, M., Su, H., Kerminen, V.-M., Petäjä, T., Tan, Z., Wang, Z., Zhou, D., Sun, J., Liao, H., Wang, H., Carslaw, K., Wood, R., Zuidema, P., Rosenfeld, D., Kulmala, M., Fu, C., … Andreae, M. O. (2021). Aerosol-boundary-layer-monsoon interactions amplify semi-direct effect of biomass smoke on low cloud formation in Southeast Asia. In Nature Communications (Vol. 12, Issue 1). Springer Science and Business Media LLC. https://doi.org/10.1038/s41467-021-26728-4

Dubovik, O., & King, M. D. (2000). A flexible inversion algorithm for retrieval of aerosol optical properties from Sun and sky radiance measurements. In Journal of Geophysical Research: Atmospheres (Vol. 105, Issue D16, pp. 20673–20696). American Geophysical Union (AGU). https://doi.org/10.1029/2000jd900282

Dubovik, O., Holben, B., Eck, T. F., Smirnov, A., Kaufman, Y. J., King, M. D., Tanré, D., & Slutsker, I. (2002). Variability of Absorption and Optical Properties of Key Aerosol Types Observed in Worldwide Locations. In Journal of the Atmospheric Sciences (Vol. 59, Issue 3, pp. 590–608). American Meteorological Society. https://doi.org/10.1175/1520-0469(2002)059<0590:voaaop>2.0.co;2

Duc, H. N., Bang, H. Q., Quan, N. H., & Quang, N. X. (2021). Impact of biomass burnings in Southeast Asia on air quality and pollutant transport during the end of the 2019 dry season. In Environmental Monitoring and Assessment (Vol. 193, Issue 9). Springer Science and Business Media LLC. https://doi.org/10.1007/s10661-021-09259-9

Dumka, U. C., Kaskaoutis, D. G., Srivastava, M. K., & Devara, P. C. S. (2015). Scattering and absorption properties of near-surface aerosol over Gangetic–Himalayan region: the role of boundary-layer dynamics and long-range transport. In Atmospheric Chemistry and Physics (Vol. 15, Issue 3, pp. 1555–1572). Copernicus GmbH. https://doi.org/10.5194/acp-15-1555-2015

Eck, T. F., Holben, B. N., Sinyuk, A., Pinker, R. T., Goloub, P., Chen, H., Chatenet, B., Li, Z., Singh, R. P., Tripathi, S. N., Reid, J. S., Giles, D. M., Dubovik, O., O'Neill, N. T., Smirnov, A., Wang, P., & Xia, X. (2010). Climatological aspects of the optical properties of fine/coarse mode aerosol mixtures. In Journal of Geophysical Research (Vol. 115, Issue D19). American Geophysical Union (AGU). https://doi.org/10.1029/2010jd014002

Engling, G., Zhang, Y.-N., Chan, C.-Y., Sang, X.-F., Lin, M., Ho, K.-F., Li, Y.-S., Lin, C.-Y., & Lee, J. J. (2011). Characterization and sources of aerosol particles over the southeastern Tibetan Plateau during the Southeast Asia biomass-burning season. In Tellus B: Chemical and Physical Meteorology (Vol. 63, Issue 1, pp. 117–128). Stockholm University Press. https://doi.org/10.1111/j.1600-0889.2010.00512.x

Fang, X., Fan, Q., Li, H., Liao, Z., Xie, J., & Fan, S. (2018). Multi-scale correlations between air quality and meteorology in the Guangdong−Hong Kong−Macau Greater Bay Area of China during 2015–2017. In Atmospheric Environment (Vol. 191, pp. 463–477). Elsevier BV. https://doi.org/10.1016/j.atmosenv.2018.08.018

Fu, J. S., Hsu, N. C., Gao, Y., Huang, K., Li, C., Lin, N.-H., & Tsay, S.-C. (2012). Evaluating the influences of biomass burning during 2006 BASE-ASIA: a regional chemical transport modeling. In Atmospheric Chemistry and Physics (Vol. 12, Issue 9, pp. 3837–3855). Copernicus GmbH. https://doi.org/10.5194/acp-12-3837-2012

Guha, A., De, B. K., Dhar, P., Banik, T., Chakraborty, M., Roy, R., Choudhury, A., Gogoi, M. M., Babu, S. S., & Moorthy, K. K. (2015). Seasonal Characteristics of Aerosol Black Carbon in Relation to Long Range Transport over Tripura in Northeast India. In Aerosol and Air Quality Research (Vol. 15, Issue 3, pp. 786–798). Taiwan Association for Aerosol Research. https://doi.org/10.4209/aaqr.2014.02.0029

Han, L., Cheng, S., Zhuang, G., Ning, H., Wang, H., Wei, W., & Zhao, X. (2015). The changes and long-range transport of PM2.5 in Beijing in the past decade. In Atmospheric Environment (Vol. 110, pp. 186–195). Elsevier BV. https://doi.org/10.1016/j.atmosenv.2015.03.013

Han, X., Zhang, M., Gao, J., Wang, S., & Chai, F. (2014). Modeling analysis of the seasonal characteristics of haze formation in Beijing. In Atmospheric Chemistry and Physics (Vol. 14, Issue 18, pp. 10231–10248). Copernicus GmbH. https://doi.org/10.5194/acp-14-10231-2014

Han, X., Zhang, M., Zhu, L., & Xu, L. (2013). Model analysis of influences of aerosol mixing state upon its optical properties in East Asia. In Advances in Atmospheric Sciences (Vol. 30, Issue 4, pp. 1201–1212). Springer Science and Business Media LLC. https://doi.org/10.1007/s00376-012-2150-4

Hansen, G. B. (2009). Calculation of single-scattering albedos: Comparison of Mie results with Hapke approximations. In Icarus (Vol. 203, Issue 2, pp. 672–676). Elsevier BV. https://doi.org/10.1016/j.icarus.2009.05.025

Haywood, J. M., & Ramaswamy, V. (1998). Global sensitivity studies of the direct radiative forcing due to anthropogenic sulfate and black carbon aerosols. In Journal of Geophysical Research: Atmospheres (Vol. 103, Issue D6, pp. 6043–6058). American Geophysical Union (AGU). https://doi.org/10.1029/97jd03426

Haywood, J. M., & Shine, K. P. (1995). The effect of anthropogenic sulfate and soot aerosol on the clear sky planetary radiation budget. In Geophysical Research Letters (Vol. 22, Issue 5, pp. 603–606). American Geophysical Union (AGU). https://doi.org/10.1029/95gl00075

Haywood, J. M., & Shine, K. P. (1997). Multi-spectral calculations of the direct radiative forcing of tropospheric sulphate and soot aerosols using a column model. In Quarterly Journal of the Royal Meteorological Society (Vol. 123, Issue 543, pp. 1907–1930). Wiley. https://doi.org/10.1002/qj.49712354307

Hu, W., Hu, M., Hu, W.-W., Zheng, J., Chen, C., Wu, Y., & Guo, S. (2017). Seasonal variations in high time-resolved chemical compositions, sources, and evolution of atmospheric submicron aerosols in the megacity Beijing. In Atmospheric Chemistry and Physics (Vol. 17, Issue 16, pp. 9979–10000). Copernicus GmbH. https://doi.org/10.5194/acp-17-9979-2017

Huang, C., Meng, L., He, Y., Shang, N., Yu, H., Huang, T., Zhu, A., Yang, H., Zhao, K., & Yao, L. (2022). Spatial variation of particulate black carbon, and its sources in a large eutrophic urban lake in China. In Science of The Total Environment (Vol. 803, p. 150057). Elsevier BV. https://doi.org/10.1016/j.scitotenv.2021.150057

Huang, K., Fu, J. S., Hsu, N. C., Gao, Y., Dong, X., Tsay, S.-C., & Lam, Y. F. (2013). Impact assessment of biomass burning on air quality in Southeast and East Asia during BASE-ASIA. In Atmospheric Environment (Vol. 78, pp. 291–302). Elsevier BV. https://doi.org/10.1016/j.atmosenv.2012.03.048

Huang, X., Ding, A., Wang, Z., Ding, K., Gao, J., Chai, F., & Fu, C. (2020). Amplified transboundary transport of haze by aerosol–boundary layer interaction in China. In Nature Geoscience (Vol. 13, Issue 6, pp. 428–434). Springer Science and Business Media LLC. https://doi.org/10.1038/s41561-020-0583-4

Jacobson, M. Z. (2000). A physically-based treatment of elemental carbon optics: Implications for global direct forcing of aerosols. In Geophysical Research Letters (Vol. 27, Issue 2, pp. 217–220). American Geophysical Union (AGU). https://doi.org/10.1029/1999gl010968

Jacobson, M. Z. (2001). Strong radiative heating due to the mixing state of black carbon in atmospheric aerosols. In Nature (Vol. 409, Issue 6821, pp. 695–697). Springer Science and Business Media LLC. https://doi.org/10.1038/35055518

Kleidman, R. G., O'Neill, N. T., Remer, L. A., Kaufman, Y. J., Eck, T. F., Tanré, D., Dubovik, O., & Holben, B. N. (2005). Comparison of Moderate Resolution Imaging Spectroradiometer (MODIS) and Aerosol Robotic Network (AERONET) remote-sensing retrievals of aerosol fine mode fraction over ocean. In Journal of Geophysical Research (Vol. 110, Issue D22). American Geophysical Union (AGU). https://doi.org/10.1029/2005jd005760

Kompalli, S. K., Babu, S. N. S., Moorthy, K. K., Satheesh, S. K., Gogoi, M. M., Nair, V. S., Jayachandran, V. N., Liu, D., Flynn, M. J., & Coe, H. (2021). Mixing state of refractory black carbon aerosol in the South Asian outflow over the northern Indian Ocean during winter. In Atmospheric Chemistry and Physics (Vol. 21, Issue 11, pp. 9173–9199). Copernicus GmbH. https://doi.org/10.5194/acp-21-9173-2021

Koulouri, E., Saarikoski, S., Theodosi, C., Markaki, Z., Gerasopoulos, E., Kouvarakis, G., Mäkelä, T., Hillamo, R., & Mihalopoulos, N. (2008). Chemical composition and sources of fine and coarse aerosol particles in the Eastern Mediterranean. In Atmospheric Environment (Vol. 42, Issue 26, pp. 6542–6550). Elsevier BV. https://doi.org/10.1016/j.atmosenv.2008.04.010

Kühn, T., Partanen, A.-I., Laakso, A., Lu, Z., Bergman, T., Mikkonen, S., Kokkola, H., Korhonen, H., Räisänen, P., Streets, D. G., Romakkaniemi, S., & Laaksonen, A. (2014). Climate impacts of changing aerosol emissions

since 1996. In Geophysical Research Letters (Vol. 41, Issue 13, pp. 4711–4718). American Geophysical Union (AGU). https://doi.org/10.1002/2014gl060349

Kumar, M., Tiwari, S., Murari, V., Singh, A. K., & Banerjee, T. (2015). Wintertime characteristics of aerosols at middle Indo-Gangetic Plain: Impacts of regional meteorology and long range transport. In Atmospheric Environment (Vol. 104, pp. 162–175). Elsevier BV. https://doi.org/10.1016/j.atmosenv.2015.01.014

Kuwata, M., Kondo, Y., Mochida, M., Takegawa, N., & Kawamura, K. (2007). Dependence of CCN activity of less volatile particles on the amount of coating observed in Tokyo. In Journal of Geophysical Research (Vol. 112, Issue D11). American Geophysical Union (AGU). https://doi.org/10.1029/2006jd007758

Lau, K. M., & Yang, S. (1997). Climatology and interannual variability of the southeast asian summer monsoon. In Advances in Atmospheric Sciences (Vol. 14, Issue 2, pp. 141–162). Springer Science and Business Media LLC. https://doi.org/10.1007/s00376-997-0016-y

Lawrence, M. G., & Lelieveld, J. (2010). Atmospheric pollutant outflow from southern Asia: a review. In Atmospheric Chemistry and Physics (Vol. 10, Issue 22, pp. 11017–11096). Copernicus GmbH. https://doi.org/10.5194/acp-10-11017-2010

Lee, H.-H., Bar-Or, R. Z., & Wang, C. (2017). Biomass burning aerosols and the low-visibility events in Southeast Asia. In Atmospheric Chemistry and Physics (Vol. 17, Issue 2, pp. 965–980). Copernicus GmbH. https://doi.org/10.5194/acp-17-965-2017

Lee, S.-Y., & Wang, C. (2015). The Response of the South Asian Summer Monsoon to Temporal and Spatial Variations in Absorbing Aerosol Radiative Forcing. In Journal of Climate (Vol. 28, Issue 17, pp. 6626–6646). American Meteorological Society. https://doi.org/10.1175/jcli-d-14-00609.1

Li, J., Zhang, G., Guo, L., Xu, W., Li, X., Lee, C. S. L., Ding, A., & Wang, T. (2007). Organochlorine pesticides in the atmosphere of Guangzhou and Hong Kong: Regional sources and long-range atmospheric transport. In Atmospheric Environment (Vol. 41, Issue 18, pp. 3889–3903). Elsevier BV. https://doi.org/10.1016/j.atmosenv.2006.12.052

Li, P., Xiao, C., Feng, Z., Li, W., & Zhang, X. (2020). Occurrence frequencies and regional variations in Visible Infrared Imaging Radiometer Suite (VIIRS) global active fires. In Global Change Biology (Vol. 26, Issue 5, pp. 2970–2987). Wiley. https://doi.org/10.1111/gcb.15034

Li, X., Cohen, J. B., Qin, K., Geng, H., Wu, L., Wu, X., Yang, C., Zhang, R., and Zhang L. (2022) Mass-Conserving Inversion of NOx Emissions and Inferred Combustion Technologies in Energy Rich Northern China Based on Multi-Year Daily Remotely Sensed and Continuous Surface Measurements. *[PREPRINT] ESSOAr*. https://doi.org/10.1002/essoar.10512337.1

Qin K., Shi J., He Q., Deng W., Wang S., Liu, J., Cohen, J. B. (2022) New Model-Free Daily Inversion of NOx Emissions using TROPOMI (MCMFE-NOx): Deducing a See-Saw of Halved Well Regulated Sources and Doubled New Sources. *[PREPRINT] ESSOAr*. https://doi.org/10.1002/essoar.10512010.1

Lin, C.-Y., Zhao, C., Liu, X., Lin, N.-H., & Chen, W.-N. (2014). Modelling of long-range transport of Southeast Asia biomass-burning aerosols to Taiwan and their radiative forcings over East Asia. In Tellus B: Chemical and Physical Meteorology (Vol. 66, Issue 1, p. 23733). Stockholm University Press. https://doi.org/10.3402/tellusb.v66.23733

Lin, C., Cohen, J. B., Wang, S., Lan, R., & Deng, W. (2020). A new perspective on the spatial, temporal, and vertical distribution of biomass burning: quantifying a significant increase in CO emissions. In Environmental Research Letters (Vol. 15, Issue 10, p. 104091). IOP Publishing. https://doi.org/10.1088/1748-9326/abaa7a

Lin, Z. J., Tao, J., Chai, F. H., Fan, S. J., Yue, J. H., Zhu, L. H., Ho, K. F., & Zhang, R. J. (2013). Impact of relative humidity and particles number size distribution on aerosol light extinction in the urban area of Guangzhou. In Atmospheric Chemistry and Physics (Vol. 13, Issue 3, pp. 1115–1128). Copernicus GmbH. https://doi.org/10.5194/acp-13-1115-2013

Liu, D., Allan, J. D., Young, D. E., Coe, H., Beddows, D., Fleming, Z. L., Flynn, M. J., Gallagher, M. W., Harrison, R. M., Lee, J., Prevot, A. S. H., Taylor, J. W., Yin, J., Williams, P. I., & Zotter, P. (2014). Size distribution, mixing state and source apportionment of black carbon aerosol in London during wintertime. In Atmospheric Chemistry and Physics (Vol. 14, Issue 18, pp. 10061–10084). Copernicus GmbH. https://doi.org/10.5194/acp-14-10061-2014

Liu, H., Chang, W. L., Oltmans, S. J., Chan, L. Y., & Harris, J. M. (1999). On springtime high ozone events in the lower troposphere from Southeast Asian biomass burning. In Atmospheric Environment (Vol. 33, Issue 15, pp. 2403–2410). Elsevier BV. https://doi.org/10.1016/s1352-2310(98)00357-4

Liu, J., & Cohen, J. (2022). Quantifying the Missing Half of Daily NOx Emissions over South, Southeast and East Asia. Research Square Platform LLC. https://doi.org/10.21203/rs.3.rs-1613262/v1

Liu, J., Chu, B., Chen, T., Liu, C., Wang, L., Bao, X., & He, H. (2018). Secondary Organic Aerosol Formation from Ambient Air at an Urban Site in Beijing: Effects of OH Exposure and Precursor Concentrations. In Environmental Science & Technology (Vol. 52, Issue 12, pp. 6834–6841). American Chemical Society (ACS). https://doi.org/10.1021/acs.est.7b05701

Liu, J., Fan, S., Horowitz, L. W., & Levy, H., II. (2011). Evaluation of factors controlling long-range transport of black carbon to the Arctic. In Journal of Geophysical Research (Vol. 116, Issue D4). American Geophysical Union (AGU). https://doi.org/10.1029/2010jd015145

Liu, J., Wang, P., Zhang, H., Du, Z., Zheng, B., Yu, Q., Zheng, G., Ma, Y., Zheng, M., Cheng, Y., Zhang, Q., & He, K. (2020). Integration of field observation and air quality modeling to characterize Beijing aerosol in different seasons. In Chemosphere (Vol. 242, p. 125195). Elsevier BV. https://doi.org/10.1016/j.chemosphere.2019.12519

Logan, J. A., Megretskaia, I., Nassar, R., Murray, L. T., Zhang, L., Bowman, K. W., Worden, H. M., & Luo, M. (2008). Effects of the 2006 El Niño on tropospheric composition as revealed by data from the Tropospheric Emission Spectrometer (TES). In Geophysical Research Letters (Vol. 35, Issue 3). American Geophysical Union (AGU). https://doi.org/10.1029/2007gl031698

Logan, T., Xi, B., Dong, X., Li, Z., & Cribb, M. (2013). Classification and investigation of Asian aerosol absorptive properties. In Atmospheric Chemistry and Physics (Vol. 13, Issue 4, pp. 2253–2265). Copernicus GmbH. https://doi.org/10.5194/acp-13-2253-2013

Lu, Z., Zhang, Q., & Streets, D. G. (2011). Sulfur dioxide and primary carbonaceous aerosol emissions in China and India, 1996–2010. In Atmospheric Chemistry and Physics (Vol. 11, Issue 18, pp. 9839–9864). Copernicus GmbH. https://doi.org/10.5194/acp-11-9839-2011

Martins, J. V., Artaxo, P., Liousse, C., Reid, J. S., Hobbs, P. V., & Kaufman, Y. J. (1998). Effects of black carbon content, particle size, and mixing on light absorption by aerosols from biomass burning in Brazil. In Journal of Geophysical Research: Atmospheres (Vol. 103, Issue D24, pp. 32041–32050). American Geophysical Union (AGU). https://doi.org/10.1029/98jd02593

May, A. A., Lee, T., McMeeking, G. R., Akagi, S., Sullivan, A. P., Urbanski, S., Yokelson, R. J., & Kreidenweis, S. M. (2015). Observations and analysis of organic aerosol evolution in some prescribed fire smoke plumes. In Atmospheric Chemistry and Physics (Vol. 15, Issue 11, pp. 6323–6335). Copernicus GmbH. https://doi.org/10.5194/acp-15-6323-2015

McMeeking, G. R., Good, N., Petters, M. D., McFiggans, G., & Coe, H. (2011). Influences on the fraction of hydrophobic and hydrophilic black carbon in the atmosphere. In Atmospheric Chemistry and Physics (Vol. 11, Issue 10, pp. 5099–5112). Copernicus GmbH. https://doi.org/10.5194/acp-11-5099-2011

Miyakawa, T., Oshima, N., Taketani, F., Komazaki, Y., Yoshino, A., Takami, A., Kondo, Y., & Kanaya, Y. (2017). Alteration of the size distributions and mixing states of black carbon through transport in the boundary layer in east Asia. In Atmospheric Chemistry and Physics (Vol. 17, Issue 9, pp. 5851–5864). Copernicus GmbH. https://doi.org/10.5194/acp-17-5851-2017

MYHRE, G., STORDAL, F., RESTAD, K., & ISAKSEN, I. S. A. (1998). Estimation of the direct radiative forcing due to sulfate and soot aerosols. In Tellus B (Vol. 50, Issue 5, pp. 463–477). Stockholm University Press. https://doi.org/10.1034/j.1600-0889.1998.t01-4-00005.x

Peng, J., Hu, M., Guo, S., Du, Z., Zheng, J., Shang, D., Levy Zamora, M., Zeng, L., Shao, M., Wu, Y.-S., Zheng, J., Wang, Y., Glen, C. R., Collins, D. R., Molina, M. J., & Zhang, R. (2016). Markedly enhanced absorption and direct radiative forcing of black carbon under polluted urban environments. In Proceedings of the National Academy of Sciences (Vol. 113, Issue 16, pp. 4266–4271). Proceedings of the National Academy of Sciences. https://doi.org/10.1073/pnas.1602310113

Penner, J. E. (1994). Carbonaceous aerosols influencing atmospheric radiation: Black and organic carbon. Office of Scientific and Technical Information (OSTI). https://doi.org/10.2172/10118242

Penner, J. E., Chuang, C. C., & Grant, K. (1998). Climate forcing by carbonaceous and sulfate aerosols. In Climate Dynamics (Vol. 14, Issue 12, pp. 839–851). Springer Science and Business Media LLC. https://doi.org/10.1007/s003820050259

Penner, J. E., Dickinson, R. E., & O'Neill, C. A. (1992). Effects of Aerosol from Biomass Burning on the Global Radiation Budget. In Science (Vol. 256, Issue 5062, pp. 1432–1434). American Association for the Advancement of Science (AAAS). https://doi.org/10.1126/science.256.5062.1432

Pham, M., Müller, J.-F., Brasseur, G. P., Granier, C., & Mégie, G. (1995). A three-dimensional study of the tropospheric sulfur cycle. In Journal of Geophysical Research (Vol. 100, Issue D12, p. 26061). American Geophysical Union (AGU). https://doi.org/10.1029/95jd02095

1003 Prasad, P., Roja Raman, M., Venkat Ratnam, M., Chen, W.-N., Vijaya Bhaskara Rao, S., Gogoi, M. M., Kompalli,
1004 S. K., Sarat Kumar, K., & Suresh Babu, S. (2018). Characterization of atmospheric Black Carbon over a
1005 semi-urban site of Southeast India: Local sources and long-range transport. In Atmospheric Research (Vol.
1006 213, pp. 411–421). Elsevier BV. https://doi.org/10.1016/j.atmosres.2018.06.024
1007 Quinn, P. K. (2004). Aerosol optical properties measured on board theRonald H. Brownduring ACE-Asia as a
1008 function of aerosol chemical composition and source region. In Journal of Geophysical Research (Vol. 109,
1009 Issue D19). American Geophysical Union (AGU). https://doi.org/10.1029/2003jd004010
1010 Ramanathan, V., Crutzen, P. J., Kiehl, J. T., & Rosenfeld, D. (2001a). Aerosols, Climate, and the Hydrological
1011 Cycle. In Science (Vol. 294, Issue 5549, pp. 2119–2124). American Association for the Advancement of
1012 Science (AAAS). https://doi.org/10.1126/science.1064034
1013 Ramanathan, V., Crutzen, P. J., Lelieveld, J., Mitra, A. P., Althausen, D., Anderson, J., Andreae, M. O., Cantrell,
1014 W., Cass, G. R., Chung, C. E., Clarke, A. D., Coakley, J. A., Collins, W. D., Conant, W. C., Dulac, F.,
1015 Heintzenberg, J., Heymsfield, A. J., Holben, B., Howell, S., … Valero, F. P. J. (2001b). Indian Ocean
1016 Experiment: An integrated analysis of the climate forcing and effects of the great Indo-Asian haze. In
1017 Journal of Geophysical Research: Atmospheres (Vol. 106, Issue D22, pp. 28371–28398). American
1018 Geophysical Union (AGU). https://doi.org/10.1029/2001jd900133
1019 Restad, K., Isaksen, I. S. A., & Berntsen, T. K. (1998). Global distribution of sulphate in the troposphere. In
1020 Atmospheric Environment (Vol. 32, Issue 20, pp. 3593–3609). Elsevier BV. https://doi.org/10.1016/s1352-
1021 2310(98)00081-8
1022 Rinsland, C. P., Luo, M., Shephard, M. W., Clerbaux, C., Boone, C. D., Bernath, P. F., Chiou, L., & Coheur, P. F.
1023 (2008). Tropospheric emission spectrometer (TES) and atmospheric chemistry experiment (ACE)
1024 measurements of tropospheric chemistry in tropical southeast Asia during a moderate El Niño in 2006. In
1025 Journal of Quantitative Spectroscopy and Radiative Transfer (Vol. 109, Issue 10, pp. 1931–1942). Elsevier
1026 BV. https://doi.org/10.1016/j.jqsrt.2007.12.020
1027 Rupakheti, D., Adhikary, B., Praveen, P. S., Rupakheti, M., Kang, S., Mahata, K. S., Naja, M., Zhang, Q., Panday,
1028 A. K., & Lawrence, M. G. (2017). Pre-monsoon air quality over Lumbini, a world heritage site along the
1029 Himalayan foothills. In Atmospheric Chemistry and Physics (Vol. 17, Issue 18, pp. 11041–11063).
1030 Copernicus GmbH. https://doi.org/10.5194/acp-17-11041-2017
1031 Rupakheti, D., Kang, S., & Rupakheti, M. (2020). Two heavy haze events over Lumbini in southern Nepal:
1032 Enhanced aerosol radiative forcing and heating rates. In Atmospheric Environment (Vol. 236, p. 117658).
1033 Elsevier BV. https://doi.org/10.1016/j.atmosenv.2020.117658
1034 Rupakheti, D., Kang, S., Rupakheti, M., Cong, Z., Panday, A. K., & Holben, B. N. (2019). Identification of
1035 absorbing aerosol types at a site in the northern edge of Indo-Gangetic Plain and a polluted valley in the
1036 foothills of the central Himalayas. In Atmospheric Research (Vol. 223, pp. 15–23). Elsevier BV.
1037 https://doi.org/10.1016/j.atmosres.2019.03.003
1038 Sahu, L. K., & Sheel, V. (2013). Spatio-temporal variation of biomass burning sources over South and Southeast
1039 Asia. In Journal of Atmospheric Chemistry (Vol. 71, Issue 1, pp. 1–19). Springer Science and Business
1040 Media LLC. https://doi.org/10.1007/s10874-013-9275-4
1041 Saiz-Lopez, A., Borge, R., Notario, A., Adame, J. A., Paz, D. de la, Querol, X., Artíñano, B., Gómez-Moreno, F. J.,
1042 & Cuevas, C. A. (2017). Unexpected increase in the oxidation capacity of the urban atmosphere of Madrid,
1043 Spain. In Scientific Reports (Vol. 7, Issue 1). Springer Science and Business Media LLC.
1044 https://doi.org/10.1038/srep45956
1045 Salam, A., Mamoon, H. A., Ullah, Md. B., & Ullah, S. M. (2012). Measurement of the atmospheric aerosol particle
1046 size distribution in a highly polluted mega-city in Southeast Asia (Dhaka-Bangladesh). In Atmospheric
1047 Environment (Vol. 59, pp. 338–343). Elsevier BV. https://doi.org/10.1016/j.atmosenv.2012.05.024
1048 Sato, M., Hansen, J., Koch, D., Lacis, A., Ruedy, R., Dubovik, O., Holben, B., Chin, M., & Novakov, T. (2003).
1049 Global atmospheric black carbon inferred from AERONET. In Proceedings of the National Academy of
1050 Sciences (Vol. 100, Issue 11, pp. 6319–6324). Proceedings of the National Academy of Sciences.
1051 https://doi.org/10.1073/pnas.0731897100
1052 Saxena, P., & Seigneur, C. (1987). On the oxidation of SO2 to sulfate in atmospheric aerosols. In Atmospheric
1053 Environment (1967) (Vol. 21, Issue 4, pp. 807–812). Elsevier BV. https://doi.org/10.1016/0004-
1054 6981(87)90077-1
1055 Schuster, G. L. (2005). Inferring black carbon content and specific absorption from Aerosol Robotic Network
1056 (AERONET) aerosol retrievals. In Journal of Geophysical Research (Vol. 110, Issue D10). American
1057 Geophysical Union (AGU). https://doi.org/10.1029/2004jd004548

Schwarz, J. P., Gao, R. S., Spackman, J. R., Watts, L. A., Thomson, D. S., Fahey, D. W., Ryerson, T. B., Peischl, J., Holloway, J. S., Trainer, M., Frost, G. J., Baynard, T., Lack, D. A., de Gouw, J. A., Warneke, C., & Del Negro, L. A. (2008). Measurement of the mixing state, mass, and optical size of individual black carbon particles in urban and biomass burning emissions. In Geophysical Research Letters (Vol. 35, Issue 13). American Geophysical Union (AGU). https://doi.org/10.1029/2008gl033968

Shen, Z., Ming, Y., & Held, I. M. (2020). Using the fast impact of anthropogenic aerosols on regional land temperature to constrain aerosol forcing. In Science Advances (Vol. 6, Issue 32). American Association for the Advancement of Science (AAAS). https://doi.org/10.1126/sciadv.abb5297

Smith, A. J. A., & Grainger, R. G. (2014). Simplifying the calculation of light scattering properties for black carbon fractal aggregates. In Atmospheric Chemistry and Physics (Vol. 14, Issue 15, pp. 7825–7836). Copernicus GmbH. https://doi.org/10.5194/acp-14-7825-2014

Song, C. H., & Carmichael, G. R. (1999). The aging process of naturally emitted aerosol (sea-salt and mineral aerosol) during long range transport. In Atmospheric Environment (Vol. 33, Issue 14, pp. 2203–2218). Elsevier BV. https://doi.org/10.1016/s1352-2310(98)00301-x

Streets, D. G., Bond, T. C., Carmichael, G. R., Fernandes, S. D., Fu, Q., He, D., Klimont, Z., Nelson, S. M., Tsai, N. Y., Wang, M. Q., Woo, J.-H., & Yarber, K. F. (2003). An inventory of gaseous and primary aerosol emissions in Asia in the year 2000. In Journal of Geophysical Research: Atmospheres (Vol. 108, Issue D21). American Geophysical Union (AGU). https://doi.org/10.1029/2002jd003093

Sun, Y. L., Wang, Z. F., Du, W., Zhang, Q., Wang, Q. Q., Fu, P. Q., Pan, X. L., Li, J., Jayne, J., & Worsnop, D. R. (2015). Long-term real-time measurements of aerosol particle composition in Beijing, China: seasonal variations, meteorological effects, and source analysis. In Atmospheric Chemistry and Physics (Vol. 15, Issue 17, pp. 10149–10165). Copernicus GmbH. https://doi.org/10.5194/acp-15-10149-2015

Takeishi, A., & Wang, C. (2022). Radiative and microphysical responses of clouds to an anomalous increase in fire particles over the Maritime Continent in 2015. In Atmospheric Chemistry and Physics (Vol. 22, Issue 6, pp. 4129–4147). Copernicus GmbH. https://doi.org/10.5194/acp-22-4129-2022

Tan, H., Liu, L., Fan, S., Li, F., Yin, Y., Cai, M., & Chan, P. W. (2016). Aerosol optical properties and mixing state of black carbon in the Pearl River Delta, China. In Atmospheric Environment (Vol. 131, pp. 196–208). Elsevier BV. https://doi.org/10.1016/j.atmosenv.2016.02.003

Tao, J., Zhang, Z., Wu, Y., Zhang, L., Wu, Z., Cheng, P., Li, M., Chen, L., Zhang, R., & Cao, J. (2019). Impact of particle number and mass size distributions of major chemical components on particle mass scattering efficiency in urban Guangzhou in southern China. In Atmospheric Chemistry and Physics (Vol. 19, Issue 13, pp. 8471–8490). Copernicus GmbH. https://doi.org/10.5194/acp-19-8471-2019

van der Werf, G. R., Randerson, J. T., Giglio, L., Gobron, N., & Dolman, A. J. (2008). Climate controls on the variability of fires in the tropics and subtropics. In Global Biogeochemical Cycles (Vol. 22, Issue 3, p. n/a-n/a). American Geophysical Union (AGU). https://doi.org/10.1029/2007gb003122

Wan, X., Kang, S., Li, Q., Rupakheti, D., Zhang, Q., Guo, J., Chen, P., Tripathee, L., Rupakheti, M., Panday, A. K., Wang, W., Kawamura, K., Gao, S., Wu, G., & Cong, Z. (2017). Organic molecular tracers in the atmospheric aerosols from Lumbini, Nepal, in the northern Indo-Gangetic Plain: influence of biomass burning. In Atmospheric Chemistry and Physics (Vol. 17, Issue 14, pp. 8867–8885). Copernicus GmbH. https://doi.org/10.5194/acp-17-8867-2017

Wang, C. (2015). Anthropogenic aerosols and the distribution of past large-scale precipitation change. In Geophysical Research Letters (Vol. 42, Issue 24). American Geophysical Union (AGU). https://doi.org/10.1002/2015gl066416

Wang, C., Jeong, G. R., & Mahowald, N. (2009) Particulate absorption of solar radiation: anthropogenic aerosols vs. dust. In Atmospheric Chemistry and Physics (Vol. 9, Issue 12, pp. 3935–3945). Copernicus GmbH. https://doi.org/10.5194/acp-9-3935-2009, 2009

Wang, J., Ge, C., Yang, Z., Hyer, E. J., Reid, J. S., Chew, B.-N., Mahmud, M., Zhang, Y., & Zhang, M. (2013). Mesoscale modeling of smoke transport over the Southeast Asian Maritime Continent: Interplay of sea breeze, trade wind, typhoon, and topography. In Atmospheric Research (Vol. 122, pp. 486–503). Elsevier BV. https://doi.org/10.1016/j.atmosres.2012.05.009

Wang, S., Cohen, J. B., Deng, W., Qin, K., & Guo, J. (2021). Using a New Top-Down Constrained Emissions Inventory to Attribute the Previously Unknown Source of Extreme Aerosol Loadings Observed Annually in the Monsoon Asia Free Troposphere. In Earth's Future (Vol. 9, Issue 7). American Geophysical Union (AGU). https://doi.org/10.1029/2021ef002167

Wang, S., Cohen, J. B., Lin, C., & Deng, W. (2020). Constraining the relationships between aerosol height, aerosol optical depth and total column trace gas measurements using remote sensing and models. In Atmospheric

Chemistry and Physics (Vol. 20, Issue 23, pp. 15401–15426). Copernicus GmbH. https://doi.org/10.5194/acp-20-15401-2020

Wang, X., Heald, C. L., Ridley, D. A., Schwarz, J. P., Spackman, J. R., Perring, A. E., Coe, H., Liu, D., & Clarke, A. D. (2014). Exploiting simultaneous observational constraints on mass and absorption to estimate the global direct radiative forcing of black carbon and brown carbon. In Atmospheric Chemistry and Physics (Vol. 14, Issue 20, pp. 10989–11010). Copernicus GmbH. https://doi.org/10.5194/acp-14-10989-2014

Wang, Y. Q. (2004). The transport pathways and sources of PM10pollution in Beijing during spring 2001, 2002 and 2003. In Geophysical Research Letters (Vol. 31, Issue 14). American Geophysical Union (AGU). https://doi.org/10.1029/2004gl019732

Webster, P. J., & Yang, S. (1992). Monsoon and Enso: Selectively Interactive Systems. In Quarterly Journal of the Royal Meteorological Society (Vol. 118, Issue 507, pp. 877–926). Wiley. https://doi.org/10.1002/qj.49711850705

Wu, J., Fu, C., Xu, Y., Tang, J. P., Wang, W., & Wang, Z. (2008). Simulation of direct effects of black carbon aerosol on temperature and hydrological cycle in Asia by a Regional Climate Model. In Meteorology and Atmospheric Physics (Vol. 100, Issues 1–4, pp. 179–193). Springer Science and Business Media LLC. https://doi.org/10.1007/s00703-008-0302-y

Xie, R., & Fang, X. (2019). The unusual 2014–2016 El Niño events: Dynamics, prediction and enlightenments. In Science China Earth Sciences (Vol. 63, Issue 5, pp. 626–633). Springer Science and Business Media LLC. https://doi.org/10.1007/s11430-019-9561-2

Xu, W. Q., Sun, Y. L., Chen, C., Du, W., Han, T. T., Wang, Q. Q., Fu, P. Q., Wang, Z. F., Zhao, X. J., Zhou, L. B., Ji, D. S., Wang, P. C., & Worsnop, D. R. (2015). Aerosol composition, oxidation properties, and sources in Beijing: results from the 2014 Asia-Pacific Economic Cooperation summit study. In Atmospheric Chemistry and Physics (Vol. 15, Issue 23, pp. 13681–13698). Copernicus GmbH. https://doi.org/10.5194/acp-15-13681-2015

Xu, X., Xie, J., Li, Y., Miao, S., & Fan, S. (2022). Measurement report: Vehicle-based multi-lidar observational study of the effect of meteorological elements on the three-dimensional distribution of particles in the western Guangdong–Hong Kong–Macao Greater Bay Area. In Atmospheric Chemistry and Physics (Vol. 22, Issue 1, pp. 139–153). Copernicus GmbH. https://doi.org/10.5194/acp-22-139-2022

Yang, S., & Lau, W. K.-M. (n.d.). Interannual variability of the Asian monsoon. In Springer Praxis Books (pp. 259–293). Springer Berlin Heidelberg. https://doi.org/10.1007/3-540-37722-0_6

Yang, Y., Liao, H., & Li, J. (2014). Impacts of the East Asian summer monsoon on interannual variations of summertime surface-layer ozone concentrations over China. In Atmospheric Chemistry and Physics (Vol. 14, Issue 13, pp. 6867–6879). Copernicus GmbH. https://doi.org/10.5194/acp-14-6867-2014

Yao, C., Yang, S., Qian, W., Lin, Z., & Wen, M. (2008). Regional summer precipitation events in Asia and their changes in the past decades. In Journal of Geophysical Research (Vol. 113, Issue D17). American Geophysical Union (AGU). https://doi.org/10.1029/2007jd009603

Yen, M.-C., Peng, C.-M., Chen, T.-C., Chen, C.-S., Lin, N.-H., Tzeng, R.-Y., Lee, Y.-A., & Lin, C.-C. (2013). Climate and weather characteristics in association with the active fires in northern Southeast Asia and spring air pollution in Taiwan during 2010 7-SEAS/Dongsha Experiment. In Atmospheric Environment (Vol. 78, pp. 35–50). Elsevier BV. https://doi.org/10.1016/j.atmosenv.2012.11.015

Yu, X., Zhu, B., & Zhang, M. (2009). Seasonal variability of aerosol optical properties over Beijing. In Atmospheric Environment (Vol. 43, Issue 26, pp. 4095–4101). Elsevier BV. https://doi.org/10.1016/j.atmosenv.2009.03.061.

Zamora, M.L., Peng, J., Hu, M., Guo, S., Marrero-Ortiz, W., Shang, D., Zheng, J., Du, Z., Wu, Z., & Zhang, R. (2019)_Wintertime aerosol properties in Beijing. In Atmospheric Chemistry and Physics (Vol. 19, Issue 22, pp. 14329–14338). Copernicus GmbH. https://doi.org/10.5194/acp-19-14329-14338.

Zhang, H., Wang, Z., Guo, P., & Wang, Z. (2009). A modeling study of the effects of direct radiative forcing due to carbonaceous aerosol on the climate in East Asia. In Advances in Atmospheric Sciences (Vol. 26, Issue 1, pp. 57–66). Springer Science and Business Media LLC. https://doi.org/10.1007/s00376-009-0057-

Zhang, J., Liu, J., Tao, S., & Ban-Weiss, G. A. (2015). Long-range transport of black carbon to the Pacific Ocean and its dependence on aging timescale. In Atmospheric Chemistry and Physics (Vol. 15, Issue 20, pp. 11521–11535). Copernicus GmbH. https://doi.org/10.5194/acp-15-11521-2015

Zhang, R., Jing, J., Tao, J., Hsu, S.-C., Wang, G., Cao, J., Lee, C. S. L., Zhu, L., Chen, Z., Zhao, Y., & Shen, Z. (2013). Chemical characterization and source apportionment of PM_{2.5} in Beijing: seasonal perspective. In Atmospheric

Chemistry and Physics (Vol. 13, Issue 14, pp. 7053–7074). Copernicus GmbH. https://doi.org/10.5194/acp-13-7053-2013

Zhang, R., Peng, J., Wang, Y., & Hu, M. (2016). Reply to Boucher et al.: Rate and timescale of black carbon aging regulate direct radiative forcing. In Proceedings of the National Academy of Sciences (Vol. 113, Issue 35). Proceedings of the National Academy of Sciences. https://doi.org/10.1073/pnas.1610241113

Zhang, Z., Shen, Y., Li, Y., Zhu, B., & Yu, X. (2017). Analysis of extinction properties as a function of relative humidity using a <i>κ</i>-EC-Mie model in Nanjing. In Atmospheric Chemistry and Physics (Vol. 17, Issue 6, pp. 4147–4157). Copernicus GmbH. https://doi.org/10.5194/acp-17-4147-2017

Zheng, M., Salmon, L. G., Schauer, J. J., Zeng, L., Kiang, C. S., Zhang, Y., & Cass, G. R. (2005). Seasonal trends in PM2.5 source contributions in Beijing, China. In Atmospheric Environment (Vol. 39, Issue 22, pp. 3967–3976). Elsevier BV. https://doi.org/10.1016/j.atmosenv.2005.03.036

Zhu, J., Liao, H., & Li, J. (2012). Increases in aerosol concentrations over eastern China due to the decadal-scale weakening of the East Asian summer monsoon. In Geophysical Research Letters (Vol. 39, Issue 9, p. n/a-n/a). American Geophysical Union (AGU). https://doi.org/10.1029/2012gl051428